

# Scaling behavior of knotted random polygons and self-avoiding polygons: Topological swelling with enhanced exponent

Erica Uehara and Tetsuo Deguchi

September 14, 2021

Department of Physics, Faculty of Core Research, Ochanomizu University  
2-1-1 Ohtsuka, Bunkyo-ku, Tokyo 112-8610, Japan

## Abstract

We show that the average size of self-avoiding polygons (SAP) with a fixed knot is much larger than that of no topological constraint if the excluded volume is small and the number of segments is large. We call it topological swelling. We argue an “enhancement” of the scaling exponent for random polygons with a fixed knot. We study them systematically through SAP consisting of hard cylindrical segments with various different values of the radius of segments. Here we mean by the average size the mean-square radius of gyration. Furthermore, we show numerically that the equilibrium length of a composite knot is given by the sum of those of all constituent prime knots. Here we define the equilibrium length of a knot by such a number of segments that topological entropic repulsions are balanced with the knot complexity in the average size. The additivity suggests the local knot picture.

# 1 Introduction

Ring polymers in solution have attracted much interest in various branches of science [1, 2, 3]. Ring polymers with trivial topology are observed in nature such as circular DNA [4], while circular DNA with nontrivial knot types are derived in experiments [5, 6]. Topological structures related to knots or pseudo-knots have been discussed in association with protein folding [7, 8]. Naturally occurring proteins whose ends connected to give a circular topology has been recently discovered [9]. Fractions of knotted species in synthesized DNA have been measured in experiments of DNA [10, 11] and recently in solid-state nanopores [12]. Furthermore, a molecular knot with eight crossings in nanoscale has been successfully synthesized [13]. Due to novel developments of experiments in chemistry, ring polymers are now effectively synthesized [14, 15, 16, 17, 18, 19, 20].

We investigate statistical properties of knotted ring polymers in a theta solvent and those in a good solvent through simulations of such random polygons (RP) and self-avoiding polygons (SAP) under the topological constraint of being equivalent to a knot, respectively. Entropic swelling occurs for the RP under a topological constraint: The average size of the RP with a fixed knot is much larger than that of no topological constraint if the number of segments  $N$  is large [21, 22, 23, 24, 25, 26]. For SAP it occurs if the excluded volume is small and segment number  $N$  is large [27, 28]. We call such entropic swelling topological swelling [27, 28]. It has been argued that it is due to entropic repulsions among segments of such RP or SAP with a knot, which were first suggested by des Cloizeaux [29]. Here we denote by the average size the mean-square radius of gyration. It was shown in an experiment that the  $g$ -factors of ring polystyrenes, which are defined as the ratios of the mean-square gyration radii of ring polymers to those of corresponding linear polymers, are in theta solvents larger than the standard theoretical value and addressed that it is due to topological effects [30].

In topological swelling, it is fundamental to evaluate the scaling exponent for the RP and SAP with a fixed knot. For knotted SAP it is confirmed that the scaling exponent is given by that of self-avoiding walks (SAW) [28], i.e., the exponent does not change. For knotted RP it is suggested in many simulations that the scaling exponent should be given by that of SAW [24, 25, 26], i.e., it should be enhanced due to topological swelling. However, it is not trivial to evaluate it numerically. It is practically hard to calculate knot invariants for polygons with large segment numbers  $N$ , and hence segment number  $N$  is limited in the simulations and not large enough to confirm the scaling behavior over three decades such as from  $N = 10^2$  to  $10^5$ . It is therefore not clear yet whether the scaling exponent of the RP with a fixed knot is equal to that of SAW.

In the paper we study the scaling exponent of the RP with a fixed knot systematically through the results of SAP by changing the excluded volume and those of the knotting probability. We demonstrate that the finite-size effect is significant in topological swelling both for RP and SAP and it is indeed not trivial to estimate the scaling exponent in simulation. However, by deriving good fitted curves to the plots of the average size versus segment number  $N$  for various values of excluded volume we argue that the estimate of the scaling exponent of the SAP with a fixed knot approaches that of SAW even for zero thickness, i.e. for the RP, as the upper limit in the plot range of  $N$  goes to infinity.

We introduce SAP consisting of  $N$  impenetrable cylindrical segments with radius  $r_{\text{ex}}$  where the segments do not overlap each other except for neighboring

ones. It gives a model of semi-flexible ring polymers such as circular DNA [10, 11]. We show that the scale of topological finite-size effect in segment number  $N$  is given by the characteristic length of the knotting probability. In the cylindrical SAP it increases exponentially as a function of the excluded-volume parameter  $r_{\text{ex}}$  and can be very large [31, 32]. Therefore, the plots of the average size of SAP with a fixed knot against  $N$  do not completely show the asymptotic behavior even for large segment numbers such as  $N = 10^4$ : the finite-size effect gradually decays over the whole plot range of  $N$  for almost all SAPs investigated.

We express the nontrivial  $N$ -dependence in the average size of the RP or SAP with a fixed knot through a formula different from the standard asymptotic expression with the fixed exponent: We show that a three-parameter formula with scaling exponent as a fitting parameter gives a good approximate curve to the plot of the mean-square gyration radius of the cylindrical SAP with a fixed knot against  $N$  for any value of radius  $r_{\text{ex}}$ . We call the parameter for the scaling exponent the effective scaling exponent. Since the  $\chi^2$  values are small, the average size of the RP or SAP with a fixed knot is expressed as a function of both number  $N$  and radius  $r_{\text{ex}}$  numerically with high accuracy. Here we remark that the mean-square gyration radius of the RP with a fixed knot was evaluated in several studies [21, 23, 24, 25, 26, 27, 28, 33], and for lattice SAP with a fixed knot the asymptotic behavior of the mean-square gyration radius was studied [34]. However, such theoretical curves with small  $\chi^2$  values have not been derived, yet, that have only three parameters to fit and quite small errors in the effective scaling exponent.

We shall argue the large- $N$  scaling behavior of the RP with a knot  $K$  through responses in the effective scaling exponent  $\nu_K$  of the cylindrical SAP with the knot  $K$  as we change radius  $r_{\text{ex}}$  and the upper limit in the plot range of  $N$ . Here, we call it the maximum of  $N$ . We show that for the cylindrical SAP of no topological constraint with a small radius  $r_{\text{ex}}$  the effective scaling exponent  $\nu_{All}$  increases to the scaling exponent of SAW  $\nu_{SAW}$  very slowly as the maximum of  $N$  increases. With an approximation we suggest that for  $r_{\text{ex}} = 0.005$  the difference  $\nu_{SAW} - \nu_{All}$  is reduced to 0.01 when the maximum of  $N$  is given by  $10^8$ . We observe that effective exponents  $\nu_K$  for knots  $K$  are continuous as functions of radius  $r_{\text{ex}}$  even at  $r_{\text{ex}} = 0$ , and also that the estimates  $\nu_K$  are larger than  $\nu_{All}$  for any value of  $r_{\text{ex}}$ . We thus suggest that effective scaling exponent  $\nu_K$  of the RP with a knot  $K$  approaches  $\nu_{SAW}$  if the maximum of  $N$  is very large such as  $10^8$ .

As another aspect of topological swelling we shall show the additivity of equilibrium lengths for composite knots. We call the number  $N_{\text{eq}}$  the equilibrium length of a knot  $K$ , if the mean-square radius of gyration of such SAP of  $N_{\text{eq}}$  segments with a knot  $K$  is equal to that of such SAP of  $N_{\text{eq}}$  segments with no topological constraint. We may interpret that when the segment number is equal to the equilibrium length the average size does not change even if we remove the topological constraint on the SAP [33]. Intuitively, in the RP or SAP with a fixed knot at the equilibrium length entropic repulsions arising from the topological constraint are balanced with the complexity of the knot. Recall that the average size of knotted SAP decreases for small  $N$  if the knot is more complex. We propose a conjecture that for a composite knot  $K_1\#K_2$  which consists of knots  $K_1$  and  $K_2$ , the equilibrium length  $N_{12}$  of knot  $K_1\#K_2$  is given by the sum:  $N_{\text{eq}1} + N_{\text{eq}2}$ , where  $N_{\text{eq}j}$  are the equilibrium lengths of knots  $K_j$  for  $j = 1$  and  $2$ . For the cylindrical SAP we show that the conjecture holds for SAP, while for RP it holds but not as good as for SAP:  $N_{12}$  is smaller than the sum for RP. We shall

argue that the additivity of equilibrium lengths is consistent with the local knot picture that the knotted region in a knotted SAP is localized [35, 36, 37, 38]. It might be suggested that the knotted region is less localized in RP than in SAP.

The contents of the present paper consist of the following. In section 2 we explain numerical methods in this research. In section 3 we present several aspects of topological swelling. We first define the ratio of topological swelling for a knot  $K$  by the ratio of the mean-square radius of gyration of the RP or SAP with the knot  $K$  to that of no topological constraint. By plotting the ratio of topological swelling for several knots against segment number  $N$  we demonstrate that the finite-size effect is dominant in the plots. We show that all the data of the ratio of topological swelling are well approximated by the fitted curves derived from the three-parameter formula with an effective scaling exponent applied to various knots for many different values of cylindrical radius  $r_{\text{ex}}$ . In section 4, we show that the three-parameter formula with scaling exponent as a fitting parameter gives good fitted curves to the data points of the mean-square gyration radius of SAP with a knot  $K$ , denoted by  $\langle R_g^2 \rangle_K$ , against segment number  $N$  for various values of radius  $r_{\text{ex}}$ . We obtain good fitted curves to five prime knots and five composite knots such as  $0_1$ ,  $3_1$ ,  $4_1$ ,  $3_1\#3_1$  and  $3_1\#4_1$ , etc. Here we remark that we define a prime knot as such a knot that cannot be expressed as a product of two nontrivial knots [39]. In section 5 we argue that the effective scaling exponent  $\nu_K$  of the RP with any fixed knot  $K$  approaches the scaling exponent of SAW (i.e.,  $\nu_{\text{SAW}}=0.588$ ) if the upper limit in the plot range of segment number  $N$  goes to infinity. We point out that the topological finite-size effect is very strong, so that the estimate  $\nu_K$  of the RP with knot  $K$  is smaller than the scaling exponent of SAW  $\nu_{\text{SAW}}$  if the number of segments  $N$  is less than  $10^4$ . In section 6 we present the additivity of equilibrium lengths for several composite knots consisting of prime knots  $3_1$  and  $4_1$ . Finally, in section 7 we give concluding remarks.

## 2 Numerical methods

### 2.1 Algorithm for generating cylindrical SAP

We construct an ensemble of SAP consisting of  $N$  hard cylindrical segments with radius  $r_{\text{ex}}$  as follows [32]. First, we construct an initial polygon by an equilateral regular  $N$ -gon, where the vertices have numbers from 1 to  $N$ , consecutively. Second, we choose two vertices randomly out of the  $N$  vertices. Suppose that they are given by numbers  $p_1$  and  $p_2$ . We rotate the sub-chain between the vertices  $p_1$  and  $p_2$  around the straight line connecting them by an angle chosen randomly from 0 to  $2\pi$ . Third, we check whether the rotated subchain has any overlap with the other part of the polygon or not. If the distance between every pair of non-neighboring segments (or polygonal edges) of the polygon is larger than  $2r_{\text{ex}}$ , we find that the polygon does not have any overlap. If it has no overlap, we employ the rotated configuration as the cylindrical SAP in the next Monte-Carlo step. If it has an overlap, we employ the previous configuration of SAP before rotation in the next Monte-Carlo step. Then, we repeat this procedure many times such as  $2N$  times.

When the correlation between the initial polygon and the current polygon becomes small, we add the current polygon to the ensemble of cylindrical SAP. Repeating the procedure  $2N$  times makes the correlation small enough. We thus

suggest that if we pick up a SAP in the employed configurations every  $2N$  Monte-Carlo steps, the correlations between samples are very small and can be neglected.

## 2.2 On the number of SAPs generated in simulation

In the simulation of the present paper to each value of cylindrical radius  $r_{\text{ex}}$  we have generated  $2 \times 10^5$  polygons for  $N \leq 4000$ ,  $10^5$  polygons for  $4000 < N \leq 6000$ ,  $5 \times 10^4$  for  $6000 < N \leq 8000$ , and  $4 \times 10^4$  for  $8,000 < N \leq 10,000$ .

We remark that for  $r_{\text{ex}} = 0$  generated polygons in the cylindrical SAP model are given by equilateral random polygons.

In the present simulation the number of segments  $N$  is given from 100 to 3000 for the cylindrical SAP of zero thickness ( $r_{\text{ex}} = 0$ ), from 100 to 3000 for cylindrical SAP with  $r_{\text{ex}} = 0.005$  and  $r_{\text{ex}} = 0.01$ , from 100 to 4000 with  $r_{\text{ex}} = 0.02$ , from 100 to 5000 with  $r_{\text{ex}} = 0.03$ , from 100 to 7000 with  $r_{\text{ex}} = 0.04$ , from 100 to 8000 with  $r_{\text{ex}} = 0.05$ , from 100 to  $10^4$  with  $r_{\text{ex}} = 0.06, 0.08$  and  $0.1$ .

In order to detect the knot type of a given SAP we mainly evaluate the two knot invariants: The absolute value of the Alexander polynomial  $|\Delta_K(t)|$  evaluated at  $t = -1$  and the Vassiliev invariant of the second order  $v_2(K)$  for a knot  $K$  [40]. If a given SAP has the same values of two knot invariants as a knot  $K$ , we assume that the topology of the polygon is given by the knot  $K$ . However, for some cases we also evaluate the Vassiliev invariant of the third order, In fact, there are some known pairs of knots that have the same values of the two knot invariants. We employ the algorithm for calculating the Vassiliev invariants of the second order and the third order through the Gauss codes (or the Dowker codes) [41].

## 3 Entropic swelling of SAP with a fixed knot

### 3.1 Ratio of topological swelling

We denote the mean-square radius of gyration of the cylindrical SAP with a knot  $K$  by  $\langle R_g^2 \rangle_K$  and that of no topological constraint by  $\langle R_g^2 \rangle_{\text{All}}$ . Here we recall that the cylindrical SAP with zero radius:  $r_{\text{ex}} = 0$  correspond to equilateral RP.

In order to express topological swelling graphically let us introduce the ratio of the mean-square radius of gyration for the cylindrical SAP with a knot  $K$  to that of no topological constraint,  $\langle R_g^2 \rangle_K / \langle R_g^2 \rangle_{\text{All}}$ . We call it the ratio of topological swelling for knot  $K$ . The estimates of the ratio of topological swelling are plotted against segment number  $N$  in Figures 1, 2 and 3 for the trivial knot ( $0_1$ ), the trefoil knot ( $3_1$ ), and composite knot  $3_1 \# 3_1$ , respectively, in the case of cylindrical SAP with different values of cylindrical radius  $r_{\text{ex}}$ , in the double-logarithmic scale. They are also shown for the figure-eight knot ( $4_1$ ) in Figure S1 of section S1. Here we remark that the composite knot  $3_1 \# 3_1$  consists of two trefoil knots ( $3_1$ ).

In Figures 1, 2 and 3 if the excluded volume is small, the ratio of topological swelling is larger than 1.0. For instance, in the case of the trivial knot, the ratio of topological swelling is larger than 1.0 for all the values of the cylindrical radius, as shown in Figure 1. For nontrivial knots, it is larger than 1.0 if the cylindrical radius is small enough and the number of segments is large enough. In Figure 2 the ratio of topological swelling for radius  $r_{\text{ex}} = 0.03$  increases with respect to the

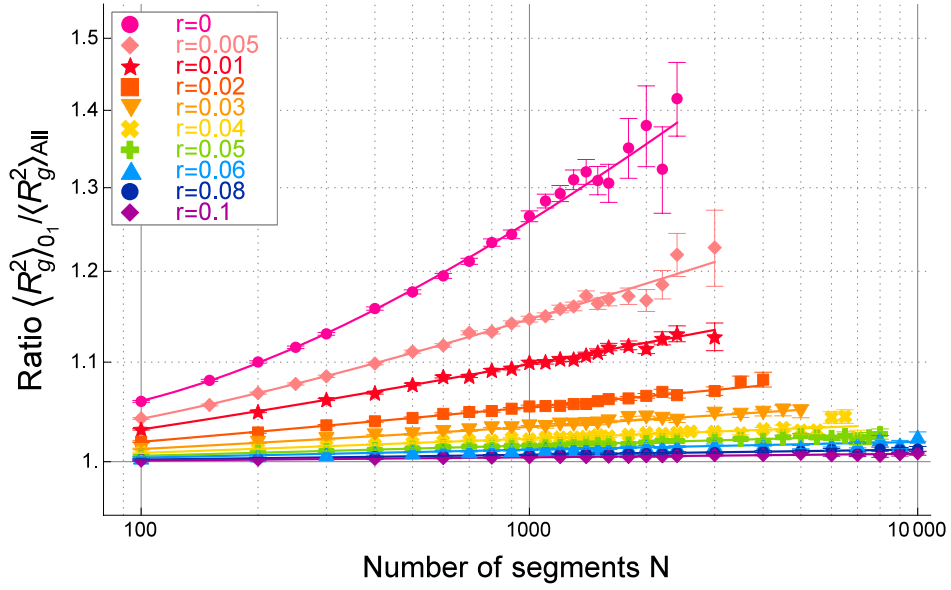


Figure 1: Ratio of topological swelling for the trivial knot ( $0_1$ ) in the cylindrical SAP with radius  $r_{ex}$ ,  $\langle R_g^2 \rangle_{0_1} / \langle R_g^2 \rangle_{All}$  plotted against the number of segments  $N$  in the double-logarithmic scale. The plots for the values of radius  $r_{ex}$  given by 0, 0.005, 0.01, 0.02, 0.03, 0.04, 0.05, 0.06, 0.08 and 0.1 are depicted by circles (red), diamonds, stars, squares, lower triangles, saltires or Xs, crosses, upper triangles, circles (blue) and diamonds (purple), respectively.

number of segments  $N$  and becomes larger than 1.0 for  $N > 1,000$  in the case of the trefoil knot ( $3_1$ ).

The finite-size effect arising from a topological constraint is significant. In the case of the trivial knot in Figure 1 for the small values of radius such as  $r_{\text{ex}} = 0.005, 0.01$  and  $0.02$  the ratio of topological swelling increases constantly with respect to the number  $N$  of segments in the double-logarithmic scale at least within the plotted range of  $N$  such as  $N \leq 4,000$ . However, if we assume that the ratio of topological swelling would increase constantly even for asymptotically large values of  $N$ , then the scaling exponent of SAP with small positive values of radius  $r_{\text{ex}}$  should be larger than that of SAW,  $\nu_{\text{SAW}}$ . Therefore, we suggest that the apparent constantly increasing behavior in the ratio of topological swelling with  $r_{\text{ex}} > 0$  in the double-logarithmic scale does not hold for asymptotically large values of  $N$ . We expect that the gradient in the graph of the ratio of topological swelling against segment number  $N$  should gradually decrease in the double-logarithmic scale as segment number  $N$  increases and finally vanish for each nonzero value of radius  $r_{\text{ex}}$ .

In the experiment [30] the  $g$ -factors,  $\langle R_g^2 \rangle_{\text{ring}} / \langle R_g^2 \rangle_{\text{linear}}$ , are evaluated from the data of the gyration radii for ring polystyrenes in  $\Theta$  solvents as  $0.557 \leq g \leq 0.730$ . They are larger than 0.5, which is the  $g$ -factor for the RP with no topological constraint and RW. If we assume that the topologies of almost all the ring polystyrenes in the experiment are given by the trivial knot, it seems that the  $g$ -factors obtained in the experiment are consistent with the theoretical estimates of the ratio of topological swelling for zero radius ( $r_{\text{ex}} = 0$ ) plotted in Figure 1.

The finite-size effect plays an important role more explicitly for nontrivial knots, as shown in Figures 2 and 3 for knots  $3_1$  and  $3_1\#3_1$ , respectively. In the case of  $r_{\text{ex}} = 0.1$  the ratio of topological swelling increases and becomes close to the value of 1.0 only when the number of segments  $N$  is very large such as  $N = 10,000$ . Here we remark that the characteristic length  $N_{0_1}$  of the knotting probability is roughly estimated by 15,000 in the case of  $r_{\text{ex}} = 0.1$  for the cylindrical SAP [32]. In Figure 2 the ratio for the trefoil knot  $3_1$  increases very slowly: it is given by 0.8 at  $N=100$ , while it becomes close to 1.0 only at  $N = 10,000$ .

For the trivial knot the finite-size correction term vanishes when the cylindrical radius  $r_{\text{ex}}$  is large [28], while for the nontrivial knots it becomes more significant as the cylindrical radius increases. It is clear in Figure 1 that the graph of the ratio versus segment number  $N$  has a more gradual rise, i.e., it increases slower, as the cylindrical radius gets larger and finally becomes almost flat. However, in Figures 2 and 3 the graphs of the ratio versus  $N$  become more bending toward the lower direction in the small  $N$  region and consequently have a sharper rise. Therefore, the finite-size effect due to a topological constraint is also significant for SAP even in the case of large excluded volume.

We suggest that the slowly increasing behavior in the plots of the ratio of topological swelling against segment number  $N$ , which is particularly clear for non-trivial knots such as shown in Figures 2 and 3, should be in agreement with the physical interpretation that we need to have a longer rope to tie a nontrivial knot if the thickness of the rope increases. Furthermore, we suggest that it corresponds to the slowly decaying behavior of the finite-size correction term in an appropriate fitting formula, which is applied to the plots of the ratio of topological swelling against segment number  $N$ .

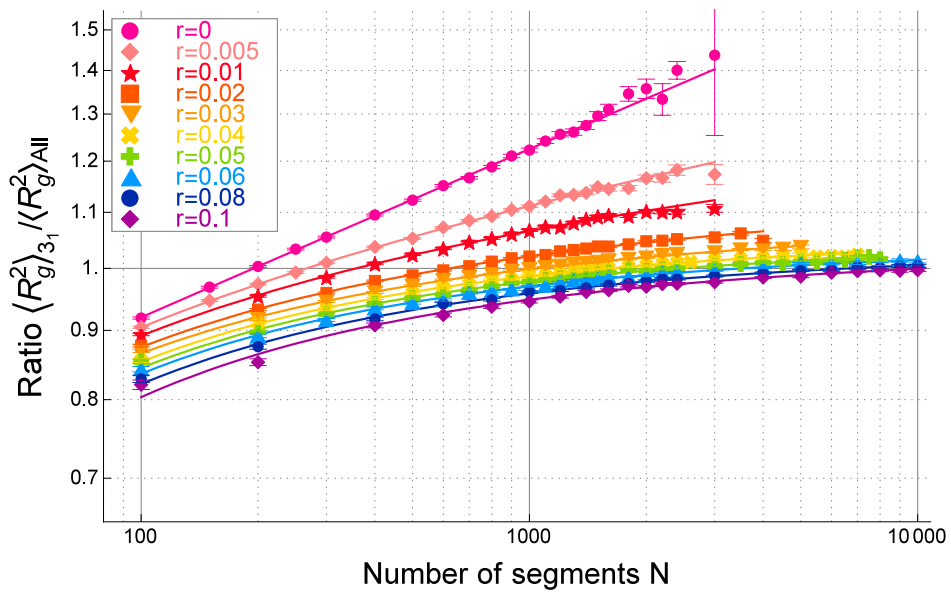


Figure 2: Ratio of topological swelling for the trefoil knot ( $3_1$ ) in the cylindrical SAP with radius  $r_{ex}$ ,  $\langle R_g^2 \rangle_{3_1} / \langle R_g^2 \rangle_{All}$  plotted against the number of segments  $N$  in the double-logarithmic scale.



We remark that topological swelling has been studied in Ref. [28] for the cylindrical SAP with several values of radius  $r_{\text{ex}}$ . However, the number of segments  $N$  was limited such as  $N \leq 10^3$  and some aspects of the finite-size effect have not been shown. In fact, the finite-size correction remains nontrivial even at  $N = 10^4$  for the cylindrical SAP with large values of the radius such as  $r_{\text{ex}} = 0.1$ , as shown in Figures 2 and 3, while it was simply expected that the ratio of topological swelling should approach 1.0 in any standard models of SAP as the number of segments  $N$  goes to infinity, if the excluded volume is large enough [28].

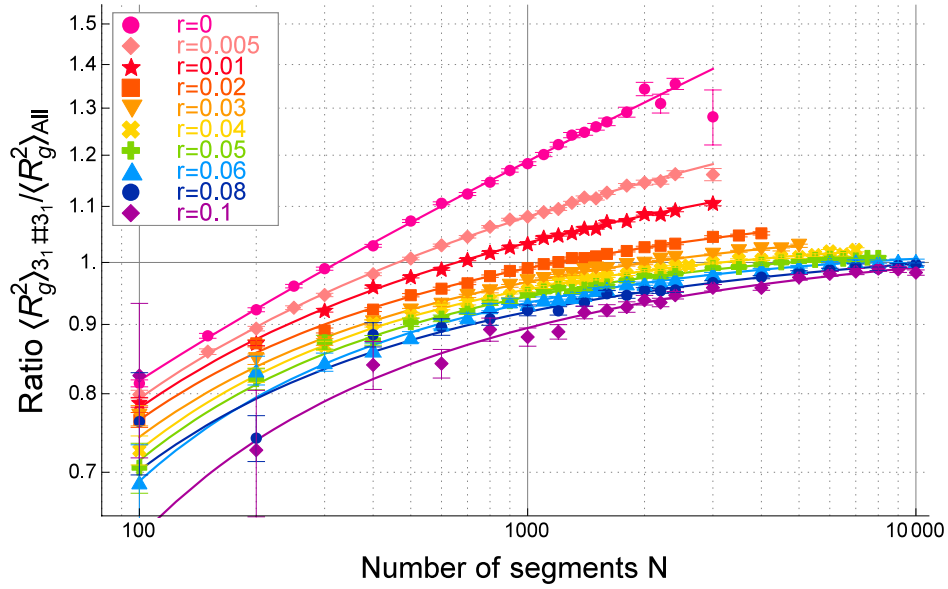


Figure 3: Ratio of topological swelling for the composite knot  $3_1 \# 3_1$  in cylindrical SAP with radius  $r_{\text{ex}}$ ,  $\langle R_g^2 \rangle_{3_1 \# 3_1} / \langle R_g^2 \rangle_{\text{All}}$ , plotted against the number of segments  $N$  in the double-logarithmic scale.

### 3.2 Three-parameter formula for the ratio of topological swelling

The finite-size effect plays an important role in the plots of the average size of SAP with a fixed knot against the number of segments  $N$  plotted in Figures 1, 2 and 3, as shown in the last subsection. It is effective almost through the whole range of the number  $N$  of segments of SAP we investigated. It follows that the

plots do not completely show the asymptotic behavior even for  $N = 10^4$ . Thus, the asymptotic expression is not necessarily appropriate to express them.

In order to express the strong finite-size effect we now introduce a three-parameter formula with scaling exponent as a fitting parameter. We also assume that the finite-size correction is proportional to the inverse square root of  $N$ .

$$\langle R_g^2 \rangle_K / \langle R_g^2 \rangle_{All} = a_K \left( 1 + \frac{b_K}{\sqrt{N}} \right) N^{2\Delta\nu_K}. \quad (1)$$

Here,  $a_K$ ,  $b_K$  and  $\Delta\nu_K$  are the fitting parameters of eq (1). We remark that the correction term corresponds to that of exponent  $\Delta_1 \approx 0.5$  in the standard asymptotic expansion of the average size of SAW (see also §4.1).

We have applied eq (1) to the plots of the ratio of topological swelling versus  $N$  for several prime knots  $0_1$ ,  $3_1$  and  $4_1$  together with some composite knots such as  $3_1\#3_1$  and  $3_1\#4_1$ . Each of the fitted curves has a small  $\chi^2$  value per degree of freedom (DF), so that they are good. The fitted curves are depicted in Figures 1, 2 and 3 (for knot  $4_1$ , see Figure S1 of section S1). We observe that they fit to the data points very well. The best estimates of knots  $0_1$ ,  $3_1$  and  $3_1\#3_1$  are listed in Tables 1, 2 and 3, respectively. For knot  $4_1$  they are given in Table S1 of section S1.

The finite-size correction term in eq (1) is appropriate to all the data shown in Figures 1, 2 and 3. In particular, the monotonically and slowly increasing behavior of the ratio of topological swelling against segment number  $N$ , shown for the non-trivial knots in 2, and 3, is very well described by the finite-size correction term of eq (1). Therefore, the fitted curves have small values of the  $\chi^2$  values per DF.

$r_{ex}$	$a_K$	$\Delta\nu_K$	$b_K$	$\chi^2/\text{DF}$
0	$0.456 \pm 0.017$	$0.0682 \pm 0.0023$	$2.39 \pm 0.19$	0.81
0.005	$0.767 \pm 0.013$	$0.0279 \pm 0.0011$	$0.502 \pm 0.080$	0.69
0.01	$0.878 \pm 0.012$	$0.01586 \pm 0.00086$	$0.155 \pm 0.061$	0.70
0.02	$0.9462 \pm 0.0071$	$0.00770 \pm 0.00047$	$0.034 \pm 0.036$	0.50
0.03	$0.9592 \pm 0.0063$	$0.00532 \pm 0.00040$	$0.048 \pm 0.032$	0.68
0.04	$0.9786 \pm 0.0049$	$0.00313 \pm 0.00030$	$0.011 \pm 0.026$	0.67
0.05	$0.9846 \pm 0.003$	$0.00224 \pm 0.00018$	$0.005 \pm 0.016$	0.35
0.06	$0.9893 \pm 0.0032$	$0.00161 \pm 0.00019$	$-0.002 \pm 0.018$	0.45
0.08	$0.9910 \pm 0.0025$	$0.00111 \pm 0.00015$	$0.007 \pm 0.014$	0.30
0.1	$0.9932 \pm 0.002$	$0.00078 \pm 0.00011$	$0.007 \pm 0.011$	0.22

Table 1: Best estimates of the parameters in eq (1) for the ratio of topological swelling for the trivial knot ( $0_1$ ),  $\langle R_g^2 \rangle_{0_1} / \langle R_g^2 \rangle_{all}$ .

In Figures 1, 2 and 3 we have observed that for the trivial knot the finite-size correction vanishes when the cylindrical radius  $r_{ex}$  is large, while for the nontrivial knots it becomes more significant as the cylindrical radius increases. We now show it by observing how the best estimates of the parameter  $b_K$  depends on the radius  $r_{ex}$ . For the trivial knot, the coefficient  $b_{0_1}$  in the finite-size correction term vanishes in the case of large values of cylindrical radius such as  $r_{ex} \geq 0.05$ , as listed in Table 1. However, for the nontrivial knots such as  $3_1$  and  $4_1$ , the

$r_{ex}$	$a_K$	$\Delta\nu_K$	$b_K$	$\chi^2/\text{DF}$
0	$0.524 \pm 0.016$	$0.0615 \pm 0.0019$	$-0.04 \pm 0.14$	0.96
0.005	$0.794 \pm 0.017$	$0.0269 \pm 0.0013$	$-1.115 \pm 0.091$	1.15
0.01	$0.911 \pm 0.020$	$0.0148 \pm 0.0013$	$-1.456 \pm 0.095$	1.76
0.02	$1.000 \pm 0.017$	$0.0054 \pm 0.0010$	$-1.681 \pm 0.082$	1.95
0.03	$1.0180 \pm 0.0085$	$0.00262 \pm 0.00049$	$-1.703 \pm 0.045$	0.66
0.04	$1.0398 \pm 0.0080$	$0.00053 \pm 0.00044$	$-1.836 \pm 0.045$	0.74
0.05	$1.035 \pm 0.010$	$0.00029 \pm 0.00055$	$-1.862 \pm 0.063$	1.3
0.06	$1.024 \pm 0.010$	$0.00049 \pm 0.00057$	$-1.875 \pm 0.067$	1.26
0.08	$1.006 \pm 0.010$	$0.00101 \pm 0.00056$	$-1.911 \pm 0.073$	0.85
0.1	$0.990 \pm 0.017$	$0.00160 \pm 0.00093$	$-2.00 \pm 0.13$	1.65

Table 2: Best estimates of the parameters in eq (1) for the ratio of topological swelling for the trefoil knot  $(3_1)$ ,  $\langle R_g^2 \rangle_{3_1} / \langle R_g^2 \rangle_{all}$ .

$r_{ex}$	$a_K$	$\Delta\nu_K$	$b_K$	$\chi^2/\text{DF}$
0	$0.496 \pm 0.023$	$0.0654 \pm 0.0029$	$-0.98 \pm 0.22$	1.30
0.005	$0.823 \pm 0.026$	$0.0253 \pm 0.0019$	$-2.37 \pm 0.14$	1.22
0.01	$0.917 \pm 0.027$	$0.0148 \pm 0.0018$	$-2.57 \pm 0.15$	1.28
0.02	$1.014 \pm 0.025$	$0.0050 \pm 0.0014$	$-2.79 \pm 0.14$	1.24
0.03	$1.038 \pm 0.024$	$0.0020 \pm 0.0013$	$-2.97 \pm 0.15$	1.18
0.04	$1.076 \pm 0.020$	$-0.0009 \pm 0.0010$	$-3.19 \pm 0.14$	0.83
0.05	$1.056 \pm 0.027$	$-0.0004 \pm 0.0013$	$-3.21 \pm 0.20$	1.11
0.06	$1.068 \pm 0.026$	$-0.0013 \pm 0.0012$	$-3.47 \pm 0.20$	0.73
0.08	$0.977 \pm 0.041$	$0.0028 \pm 0.0021$	$-3.0 \pm 0.4$	0.79
0.1	$0.969 \pm 0.081$	$0.0033 \pm 0.0042$	$-3.73 \pm 0.80$	1.06

Table 3: Best estimates of the parameters in eq (1) for the ratio of topological swelling for composite knot  $3_1 \# 3_1$ ,  $\langle R_g^2 \rangle_{3_1 \# 3_1} / \langle R_g^2 \rangle_{all}$ .

absolute value of the coefficient  $b_K$  increases for each knot as the cylindrical radius increases, as listed in Tables 2 (for knot  $4_1$  see TableS1 of section S1).

### 3.3 Characteristic length of the knotting probability and the equilibrium length of a knot

We define the knotting probability of a knot  $K$  for a model of RP or SAP by the probability that a given configuration of RP or SAP of  $N$  segments in the model has the knot type  $K$ . We denote it by  $P_K(N)$ . For a wide range of the number of segments  $N$  we can approximate the knotting probability of a knot  $K$  as a function of  $N$  as

$$P_K(N) = C_K(N - \Delta N(K))^{m(K)} \exp(-(N - \Delta N(K)) / N_K), \quad (2)$$

where  $C_K$ ,  $N_K$ ,  $m(K)$  and  $\Delta N(K)$  are fitting parameters [42, 43]. It is shown for the cylindrical SAP that the estimates  $N_K$  for many different knots  $K$  are all approximately equal to that of the trivial knot:  $N_K \approx N_{0_1}$  [31, 32]. Thus, we denote them simply by  $N_0$  [42] and call it the characteristic length of the knotting probability. The estimates of  $N_0$  for the cylindrical SAP with some values of radius  $r_{\text{ex}}$  are given in Table 4. We remark that the corrections  $\Delta N(K)$  are smaller than the characteristic length  $N_0$ , and can be neglected for large  $N$ .

In Figure 2 we observe that the ratio of topological swelling for knot  $3_1$  reaches the value 1.0 when the number of segments  $N$  is approximately equal to the characteristic length  $N_0$ . Here we recall that if the ratio of topological swelling for a knot  $K$  becomes 1.0 in the RP or SAP with a knot  $K$  of  $N$  segments, then we call the number  $N$  the equilibrium length of the knot  $K$  with respect to the mean-square radius of gyration of the RP or SAP [33]. The estimates of the equilibrium length for simple prime knots are listed in Table 4. In Figure 3 the ratio of topological swelling for composite knot  $3_1\#3_1$  reaches the value 1.0 when segment number  $N$  is approximately equal to twice the characteristic length  $N_0$ .

$r_{\text{ex}}$	$N_0$	$3_1$	$4_1$	$5_1$	$5_2$
0.0	$246 \pm 1$	$197 \pm 8$	$291 \pm 21$	$394 \pm 62$	$387 \pm 37$
0.01	$483 \pm 2$	$353 \pm 8$	$601 \pm 38$	$869 \pm 92$	$839 \pm 80$
0.02	$818 \pm 3$	$626 \pm 15$	$1119 \pm 47$	$1653 \pm 151$	$1793 \pm 127$
0.03	$1290 \pm 4$	$1036 \pm 14$	$2024 \pm 93$	$2669 \pm 240$	$2850 \pm 166$
0.04	$1966 \pm 5$	$1610 \pm 15$	$3298 \pm 108$	$4106 \pm 324$	$4820 \pm 320$
0.05	$2903 \pm 6$	$2383 \pm 29$	$5106 \pm 168$	$6386 \pm 530$	$10243 \pm 512$

Table 4: Equilibrium length  $N_{\text{eq}}$  for prime knots  $3_1$ ,  $4_1$ ,  $5_1$  and  $5_2$  and the characteristic length of the knotting probability  $N_0$  versus radius  $r_{\text{ex}}$  of cylindrical segments.

Let us confirm numerically the above observation in Figs. 2 and 3. We calculate the ratio of topological swelling,  $\langle R_g^2 \rangle_K / \langle R_g^2 \rangle_{\text{All}}$ , for a knot  $K$  through the best estimates of the parameters  $a_K$ ,  $b_K$  and  $\Delta \nu_K$  of the fitted curves given by eq (1) listed in Tables 2 and 3. For  $r_{\text{ex}} = 0.02$  the ratio for the trefoil knot  $3_1$  becomes 1.0 at  $N = 626$ , while that of the composite knot  $3_1\#3_1$  becomes 1.0 at  $N = 1244$ . It is very close to twice the number 626, which is given by 1252. The characteristic length  $N_0$  is approximately given by 820, where we have the ratio  $N_{\text{eq}}/N_0 = 626/820 \approx 0.76$ . Thus, the average size of the SAP of knot  $3_1$  is equal

to that of no topological constraint when segment number  $N$  is slightly smaller than  $N_0$ .

We now argue that the ratio of topological swelling for a composite knot consisting of  $n$  trefoil knots,  $\langle R_g^2 \rangle_{3_1 \# \dots \# 3_1} / \langle R_g^2 \rangle_{All}$ , reaches or becomes greater than 1.0 around at  $N = nN_0$ . Hereafter we denote the composite knot consisting of  $n$  trefoil knots  $3_1 \# \dots \# 3_1$  by  $K_{comp}$ .

In terms of the knotting probabilities  $P_K(N)$  the mean-square radius of gyration for SAP under no topological constraint,  $\langle R_g^2 \rangle_{All}$ , is expressed as the average of the mean-square radius of gyration for SAP with fixed knots  $\langle R_g^2 \rangle_K$  over all different knots. We classify all knots into such classes of knots consisting of  $n$  prime knots for  $n = 1, 2, \dots$ . There are prime knots ( $n = 1$ ), the composite knots consisting of two prime knots ( $n = 2$ ), etc. Here we assume that the trivial knot consists of zero prime knot ( $n = 0$ ). We recall that for a given knot  $K$  we denote the number of constituent prime knots by  $|K|$ . Then, we have

$$\langle R_g^2 \rangle_{All} = \sum_{n=0}^{\infty} \sum_{|K|=n} \langle R_g^2 \rangle_K P_K(N). \quad (3)$$

Here we assume that the symbol  $\sum_{|K|=n}$  denotes the sum over all knots consisting of  $n$  prime knots.

It follows from eq (2) that the knotting probability has the maximum value around at  $N = m(K)N_0$ . The knotting probability  $P_K(N)$  becomes quite small for  $N < m(K)N_0$  due to the power  $(N/N_0)^{m(K)}$  in eq (2) and decreases exponentially with respect to  $N$  for  $N > m(K)N_0$ . Here we remark that the exponent  $m(K)$  are close to the integers  $n$  for composite knots consisting of  $n$  prime knots [42, 43]. Thus, if the number of segments  $N$  is given by  $N = nN_0$  for some integer  $n$ , the right-hand side of eq (3), i.e., the average of the mean-square radius of gyration over all knots, is approximately given by the contribution from the knots consisting of  $n$  prime knots.

For simplicity, let us assume that simple knots consisting of  $n$  prime knots have some similar values of the mean-square radius of gyration as the given composite knot  $K_{comp}$  in common, or they are all smaller than  $K_{comp}$  with respect to size. We therefore have

$$\begin{aligned} \langle R_g^2 \rangle_{All} &\approx \sum_{|K|=n} \langle R_g^2 \rangle_K P_K(N) \\ &\approx \langle R_g^2 \rangle_{K_{comp}} \sum_{|K|=n} P_K(N) < \langle R_g^2 \rangle_{K_{comp}} \quad \text{for } N = nN_0 \end{aligned} \quad (4)$$

It follows from eq (4) that the ratio of topological swelling,  $\langle R_g^2 \rangle_{K_{comp}} / \langle R_g^2 \rangle_{All}$ , becomes greater than 1.0 around at  $N = nN_0$ .

It seems that the evaluation  $\langle R_g^2 \rangle_{K_{comp}} / \langle R_g^2 \rangle_{All} > 1$  at  $N = nN_0$  is valid, although the assumption that simple knots consisting of  $n$  prime knots have similar average sizes does not necessarily always hold. For an illustration, let us consider the  $n = 1$  case of eq (4). It is easy to see that the derivation of eq (4) is valid also for  $n = 1$ . We observe in Table 4 that the equilibrium length of knot  $3_1$  is approximately equal to but slightly smaller than the characteristic length of the knotting probability  $N_0$  for each value of radius  $r_{ex}$ . Therefore, the ratio of topological swelling is greater than 1.0 at  $N = N_0$ . We thus find that it is consistent with eq (4) in the case of  $n = 1$ .

### 3.4 Topological swelling among different knots

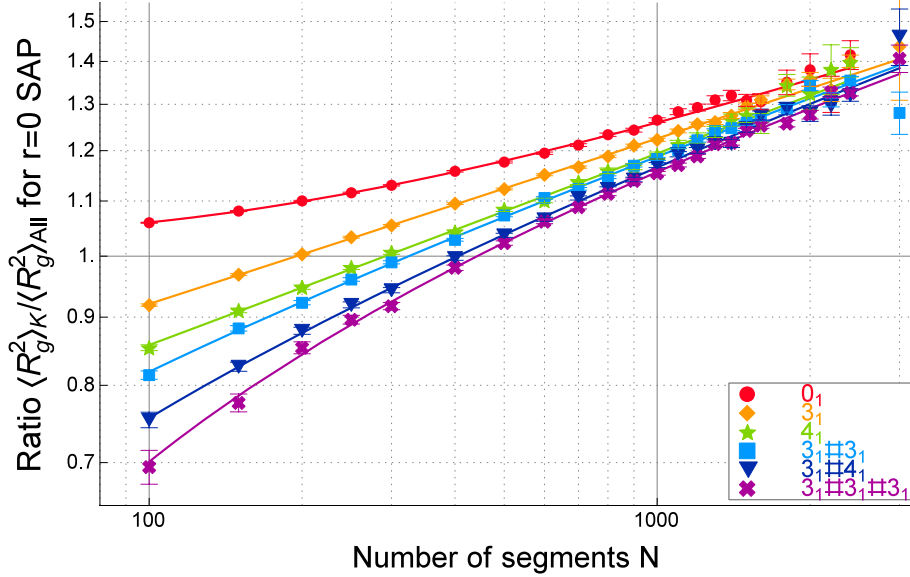


Figure 4: Ratio of topological swelling for a knot  $K$  in the equilateral RP,  $\langle R_g^2 \rangle_K / \langle R_g^2 \rangle_{All}$ , is plotted against the number of segments  $N$  for various knots  $K$  in the double-logarithmic scale. The plots for the trivial knot ( $0_1$ ), the trefoil knot ( $3_1$ ), the figure-eight knot ( $4_1$ ), and three composite knots  $3_1\#3_1$ ,  $3_1\#4_1$  and  $3_1\#3_1\#3_1$  are depicted by filled circles, diamonds, stars, squares, lower triangles and crosses, respectively, from  $N=100$  to 3000.

We expect that the mean-square radius of gyration in the cylindrical SAP with a fixed knot does not depend on the knot type if the number of segments  $N$  is very large. If the knotted region of SAP with a fixed knot is localized along the polygonal chain, the difference in the average size among different knots should vanish as the number of segments  $N$  goes to infinity.

In order to confirm it, we plot the ratio of topological swelling against segment number  $N$  for the trivial knot and some nontrivial knots. In Figure 4 the ratio of topological swelling for the different knots in the equilateral RP,  $\langle R_g^2 \rangle_K / \langle R_g^2 \rangle_{All}$ , is plotted against the number of segments  $N$ . Here it is given by the cylindrical SAP in the case of zero thickness:  $r_{ex} = 0$ . The ratio becomes larger than 1.0 for each of the six knots if segment number  $N$  is larger than 300 or 400. We observe that the ratios for the six knots become close to each other for large  $N$  such as  $N = 2,000$ .

For the equilateral random polygons the ratio of topological swelling for the trefoil knot ( $3_1$ ) becomes 1.0 at  $N = 197$ , while that of the composite knot  $3_1\#3_1$  at  $N = 325$ , which is slightly smaller than twice the number 197. Here the characteristic length  $N_0$  is approximately given by 246, where we have the ratio  $N_{\text{eq}}/N_0 = 197/246 \approx 0.80$ . Thus, for  $N = N_0$ , the ratio of topological swelling for the trefoil knot ( $3_1$ ) is larger than 1.0 as argued in eq (4). For the figure-eight knot ( $4_1$ ) the ratio of topological swelling becomes 1.0 at  $N = 291$ , which is slightly larger than  $N_0$ .

## 4 Scaling behavior of SAP with a fixed knot

### 4.1 Asymptotic expression of the mean-square radius of gyration

We first review briefly some known results on the asymptotic behavior of the average size of polymer chains with excluded volume [44, 45, 46, 47, 48]. According to the standard renormalization group (RG) arguments [45] it is predicted that the mean-square radius of gyration  $\langle R_g^2 \rangle_{\text{linear}}$  of any real polymer chain should have the asymptotic behavior

$$\langle R_g^2 \rangle_{\text{linear}} = A_L N^{2\nu_{\text{SAW}}} \left( 1 + b_L^{(1)} N^{-\Delta_1} + \dots \right), \quad (5)$$

as  $N$  increases infinitely [46]. The critical exponents  $\nu_{\text{SAW}}$  and  $\Delta_1$  are universal. The estimates  $\nu_{\text{SAW}} = 0.5880 \pm 0.0015$  and  $\Delta_1 = 0.470 \pm 0.025$  were obtained by RG arguments via the  $n = 0$  limit of the  $n$ -vector field theory model [44], while the estimates  $\nu_{\text{SAW}} = 0.5877 \pm 0.0006$  and  $\Delta_1 = 0.56 \pm 0.03$  were obtained by the simulation of three-dimensional SAWs on lattice [46].

We assume that the mean-square radius of gyration of the cylindrical SAP under no topological constraint,  $\langle R_g^2 \rangle_{\text{All}}$ , has the same asymptotic behavior as the mean-square radius of gyration of SAW, as  $N$  goes to infinity

$$\langle R_g^2 \rangle_{\text{All}} = A_R N^{2\nu_{\text{SAW}}} \left( 1 + b_R^{(1)} N^{-\Delta_1} + \dots \right). \quad (6)$$

We employ eq (6) as a fitting formula with three parameters  $A_R$ ,  $b_R^{(1)}$  and  $\Delta_1$ . By putting  $\nu_{\text{SAW}} = 0.588$  we apply eq (6) to the data of  $\langle R_g^2 \rangle_{\text{All}}$  versus  $N$  for several different values of cylindrical radius  $r_{\text{ex}}$ . The fitted curves given by eq (6) are good except for the case of  $r_{\text{ex}} = 0$ . The best estimates with  $\chi^2$  values per DF are listed in Table 5.

We suggest that the estimate of  $\Delta_1$  for the large radius case of  $r_{\text{ex}} = 0.1$  is consistent with that of SAW. In Table 5 the estimate of  $\Delta_1$  decreases as radius  $r_{\text{ex}}$  decreases. We have  $\Delta_1 = 0.426 \pm 0.032$  at  $r_{\text{ex}} = 0.10$ , which is close to the estimate  $\Delta_1 = 0.47 \pm 0.03$  derived through the  $n = 0$  limit of the field theory.

We have applied the asymptotic expression of eq (6) also to the data of the mean-square radius of gyration for the cylindrical SAP with a fixed knot  $K$  denoted by  $\langle R_g^2 \rangle_K$  versus segment number  $N$ . For the trivial knot, we have good fitted curves. For nontrivial knots, however, we do not always have good fitted curves for all values of radius  $r_{\text{ex}}$ .

For lattice SAP the asymptotic expression of eq (6) has been applied to the data of the mean-square radius of gyration under a topological constraint [34].

$r_{\text{ex}}$	$A_R$	$\Delta_1$	$b_R^{(1)}$	$\chi^2/\text{DF}$
0	$0.00200 \pm 0.00038$	$0.1929 \pm 0.003$	$43.1 \pm 8.1$	2.09
0.005	$0.01843 \pm 0.00015$	$0.2854 \pm 0.0033$	$4.284 \pm 0.012$	1.04
0.01	$0.024916 \pm 0.00009$	$0.3273 \pm 0.0031$	$3.029 \pm 0.020$	0.58
0.02	$0.03267 \pm 0.00010$	$0.3737 \pm 0.0062$	$2.088 \pm 0.041$	1.64
0.03	$0.037817 \pm 0.000078$	$0.3903 \pm 0.0064$	$1.566 \pm 0.035$	1.25
0.04	$0.042129 \pm 0.000046$	$0.4166 \pm 0.0053$	$1.300 \pm 0.026$	0.65
0.05	$0.045778 \pm 0.000039$	$0.4305 \pm 0.0058$	$1.061 \pm 0.024$	0.56
0.06	$0.048918 \pm 0.00006$	$0.4285 \pm 0.0099$	$0.843 \pm 0.033$	1.02
0.08	$0.054784 \pm 0.000054$	$0.455 \pm 0.014$	$0.599 \pm 0.034$	0.72
0.1	$0.059973 \pm 0.000089$	$0.426 \pm 0.032$	$0.308 \pm 0.038$	1.35

Table 5: Best estimates of the parameters of the asymptotic expansion (6) for the mean-square gyration radius of the cylindrical SAP with radius  $r_{\text{ex}}$  under no topological constraint  $\langle R_g^2 \rangle_{\text{All}}$ .

It was suggested that the estimate  $\Delta_1 = 1/4$  should be the most favorable to the data, although other values such as  $\Delta_1 = 1/2$  are not completely denied. Thus, the correction term in the asymptotic expansion has not been numerically determined, yet.

## 4.2 Fitting formula with an effective scaling exponent

We now introduce the effective scaling exponent through curves fitted to the data of the mean-square radius of gyration for the cylindrical SAP with a fixed knot  $K$ ,  $\langle R_g^2 \rangle_K$ , versus segment number  $N$ . We consider a three-parameter formula with a scaling exponent to be fitted where the finite-size correction is proportional to the inverse of the square root of segment number  $N$

$$\langle R_g^2 \rangle_K = A_K \left( 1 + \frac{B_K}{\sqrt{N}} \right) N^{2\nu_K}. \quad (7)$$

Here, the exponent  $\nu_K$ , the amplitude  $A_K$  and the coefficient  $B_K$  are fitting parameters. We call the parameter  $\nu_K$  the effective scaling exponent of knot  $K$ .

By applying eq (7) to the data of the mean-square radius of gyration for cylindrical SAP with a fixed knot versus segment number  $N$ , we observe that fitted curves are appropriate to the plots of all the knot types and for all the ten different values of cylindrical radius  $r_{\text{ex}}$  from 0 to 0.1, as shown in the captions. The  $\chi^2$  values per DF are small such as less than 2.0 for almost all fitted curves. For instance, the best estimates of the parameters of eq (7) with the  $\chi^2$  values for knots  $0_1$ ,  $3_1$ , and  $4_1$  are listed in Tables S2 of section S2. For other seven knots such as  $5_1$ ,  $5_2$ ,  $3_1\#3_1$ ,  $3_1\#4_1$ ,  $3_1\#3_1\#3_1$ ,  $3_1\#3_1\#4_1$ , and  $3_1\#4_1\#4_1$  the best estimates of the parameters of eq (7) are also listed in Table S3 - S7 of section S2.

The formula of eq (7) corresponds to that of eq (1) if we have good fitted curves to the plots of the mean-square radius of gyration for the cylindrical SAP under no topological constraint,  $\langle R_g^2 \rangle_{\text{All}}$ , against segment number  $N$ . The  $\chi^2$  values are not large, as given together with the best estimates of the parameters in Table S8 of section S3.



### 4.3 Finite-size correction term

It is not trivial to choose an appropriate correction term  $1/N^\Delta$ , as suggested in Ref. [49]. We therefore simply put  $\Delta = 1/2$  in eq (7). Here we remark that in the perturbative approach to the excluded-volume effect the mean-square radius of gyration of a polymer is expanded in terms of the inverse square root of segment number  $N$  [50].

If we choose other powers of  $N$  as the finite-size correction term in eq (7) such as the inverse of  $N$ , the  $\chi^2$  values per DF are not small and hence the fitted curves derived are not good. We have also applied the formula of eq (7) with no finite-size correction term, i.e. we put  $B_K = 0$ . The fitted curves are not good with respect to the  $\chi^2$  values. By applying eq (7) with  $B_K = 0$  to the data points of the mean-square gyration radius for the equilateral RP with the trivial knot ( $0_1$ ) evaluated in the plot range of  $N \leq 2400$ , we have obtained the estimate of  $\nu_0 = 0.53$ , where the  $\chi^2$  values per DF are rather large such as 18.

In the experiment it is shown that the mean-square radii of gyration of ring polystyrenes in  $\Theta$  solvents are scaled with an enhanced exponent 0.53, where the formula of eq (7) with no finite-size correction term is applied to the experimental data [30]. Thus, the estimate of the scaling exponent in the experiment coincides with that of the present research for the trivial knot if we apply eq (7) with no correction term (i.e.,  $B_K = 0$ ). We conclude that the experimental estimate of the scaling exponent [30] is not in contradiction with the theoretical estimate of the trivial knot evaluated in the present paper.

## 5 Scaling exponent of the RP with a knot

### 5.1 Continuous change in effective exponent with respect to radius

In Figure 5 the best estimates of the effective scaling exponent  $\nu_K$  for the cylindrical SAP with a knot  $K$  are plotted against cylindrical radius  $r_{\text{ex}}$  for the four knots:  $0_1$ ,  $3_1$ ,  $4_1$  and  $3_1\#3_1$ . We observe that for each knot  $K$  the estimate of  $\nu_K$  decreases very slowly as cylindrical radius  $r_{\text{ex}}$  decreases and approaches zero. In particular, the change of the effective scaling exponent  $\nu_K$  near the origin at  $r_{\text{ex}} = 0$  is rather small. On the other hand, the effective scaling exponent of the cylindrical SAP under no topological constraint,  $\nu_{\text{All}}$ , abruptly decreases near the origin at  $r_{\text{ex}} = 0$  as cylindrical radius  $r_{\text{ex}}$  decreases and approaches zero. We have  $\nu_{\text{All}} = 0.5$  at  $r_{\text{ex}} = 0$ , while we have  $\nu_{\text{All}} = 0.55$  for a small nonzero radius of  $r_{\text{ex}} = 0.005$ .

We thus propose a conjecture that the effective scaling exponent  $\nu_K$  of the cylindrical SAP with radius  $r_{\text{ex}}$  of any given knot  $K$  should be continuous as a function of cylindrical radius  $r_{\text{ex}}$  particularly near the origin of  $r_{\text{ex}} = 0$ .

Even in the case of zero radius (i.e.,  $r_{\text{ex}} = 0$ ), the effective scaling exponent  $\nu_K$  of a knot  $K$  is definitely larger than 0.5. We observe such enhancement of the effective scaling exponent  $\nu_K$  clearly in Figure 5. Here, the scaling exponent of RW and RP is given by 0.5, and we denote it by  $\nu_{\text{RW}}$ . The estimates of  $\nu_K$  at  $r_{\text{ex}} = 0$  are distinct from the value of  $\nu_{\text{RW}}$  with respect to error bars which are given by the standard deviations. We have thus described topological swelling for random knots in terms of the effective scaling exponent  $\nu_K$ .

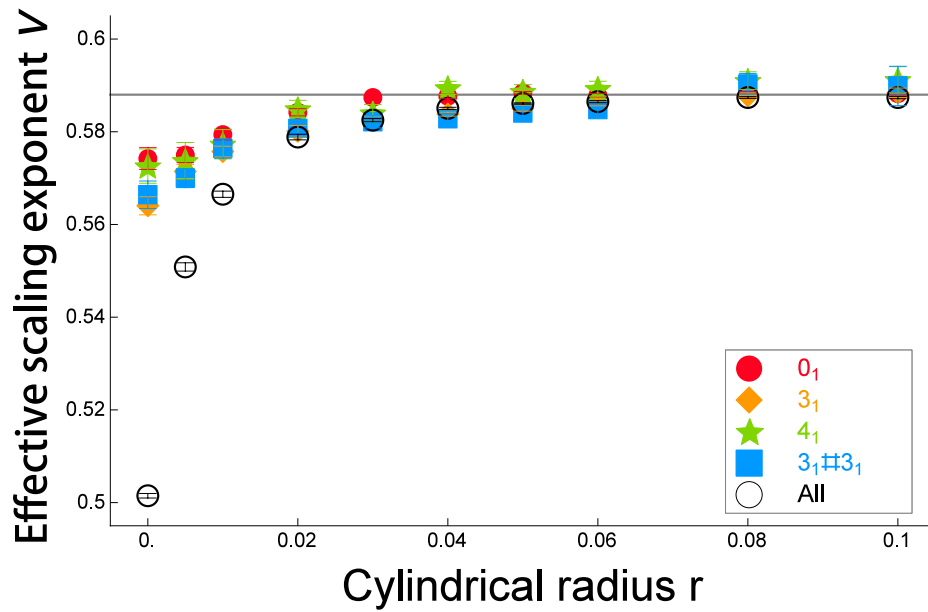


Figure 5: Best estimates of effective scaling exponent  $\nu_K$  defined by eq (7) for the mean-square radius of gyration of the cylindrical SAP with a knot  $K$  versus radius  $r_{\text{ex}}$  of cylindrical segments in the case of the trivial, trefoil, figure-eight knots and composite knot  $3_1\#3_1$  are depicted by filled crosses, circles, diamonds, and squares, respectively. Those of SAP under no topological constraint  $\nu_{\text{All}}$  (All) are depicted by open circles.

The effective scaling exponent  $\nu_K$  for the equilateral RP with a knot  $K$  is distinctly smaller than that of SAW,  $\nu_{\text{SAW}} = 0.588$ , with respect to errors, as shown in Figure 5. The estimates  $\nu_K$  for some knots are evaluated in the plot range of  $N$  with the upper limit of  $N = 3,000$ . For zero radius ( $r_{\text{ex}} = 0$ ) the estimates  $\nu_K$  of the trivial and the trefoil knots are given by  $\nu_{0_1} = 0.574 \pm 0.002$  and  $\nu_{3_1} = 0.563 \pm 0.002$ , respectively. They are listed in Table S2 of section S2.

## 5.2 Enhancement in effective scaling exponent of the RP with a knot

We now argue that the effective scaling exponent  $\nu_K$  of the equilateral RP with a knot  $K$  approaches the scaling exponent of SAW:  $\nu_{\text{SAW}} = 0.588$ , if the upper limit in the plot range of segment number  $N$  goes to infinity. Hereafter, we call the upper limit in the plot range of  $N$  the maximum segment number  $N$  or the maximum of  $N$ , in brief.

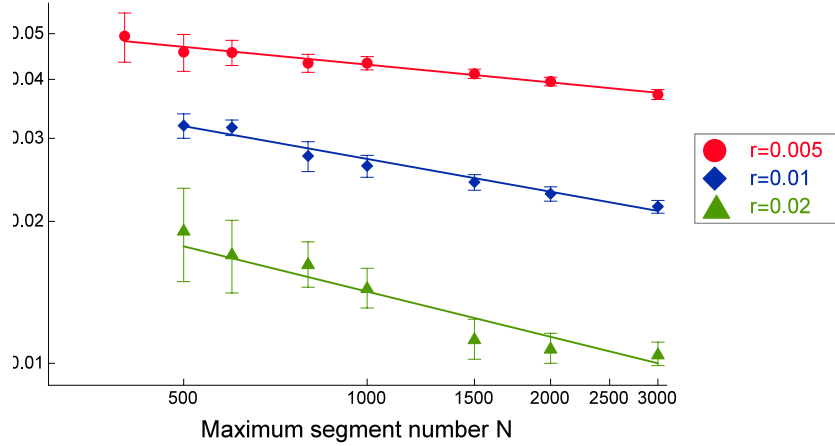


Figure 6: Difference of effective scaling exponent  $\nu_{All}$  to scaling exponent of SAW  $\nu_{\text{SAW}}$ :  $\nu_{\text{SAW}} - \nu_{All}$  versus maximum segment number  $N$  (i.e., the upper limit of the plot range of  $N$ ) in the double-logarithmic scale. The plots of  $r_{\text{ex}} = 0.005, 0.01$  and  $0.02$  are depicted by filled circles, diamonds and upper triangles, respectively. Here we put  $\nu_{\text{SAW}} = 0.588$ .

Let us assume that for any small value of the excluded volume the effective scaling exponent of SAW approaches the value of  $\nu_{\text{SAW}}$  if the maximum segment number  $N$  becomes very large. For instance, the effective exponent  $\nu_{All}$  defined

by eq (7) for the cylindrical SAP under no topological constraint (i.e.,  $K = All$ ) with radius  $r_{\text{ex}} = 0.01$  is given by  $\nu_{All} = 0.5665 \pm 0.0007$  evaluated in the plot range from  $N = 100$  to  $N = 3,000$ . However, we expect that if we increase the maximum segment number  $N$  to a very large number for the cylindrical SAP with  $r_{\text{ex}} = 0.01$ , then the effective scaling exponent  $\nu_{All}$  should increase and become much closer to the value of  $\nu_{\text{SAW}} = 0.588$ . Here we remark that the estimates  $\nu_{All}$  for other values of cylindrical radius  $r_{\text{ex}}$  are listed in Table S8 of section S3.

In Figure 6, the difference between the effective scaling exponent  $\nu_{All}$  and the scaling exponent of SAW  $\nu_{\text{SAW}}$  is plotted against the upper limit in the plot range of segment number  $N$  for the cylindrical SAP in the case of radius  $r_{\text{ex}} = 0.005$ , 0.01 and 0.02, respectively, in the double-logarithmic scale. We observe that the plots can be approximated by linear lines in all the three cases. We also observe in Figure 6 that the absolute value of the gradient of the fitted line increases as the cylindrical radius becomes larger: the more the excluded volume is, the faster  $\nu_{All}$  approaches  $\nu_{\text{SAW}}$ .

In the case of  $r_{\text{ex}} = 0.005$  the fitted line is the best among the three cases of values of radius  $r_{\text{ex}}$ . We suggest that the effective scaling exponent  $\nu_{All}$  approaches the scaling exponent of SAW where the difference of exponents:  $\nu_{\text{SAW}} - \nu_{All}$  is roughly approximated by the inverse power of  $N$  with a small exponent such as 0.125 with a constant  $c_{All}$ :

$$\nu_{All} = \nu_{\text{SAW}} - c_{All}N^{-0.125}. \quad (8)$$

Thus, it approaches  $\nu_{\text{SAW}}$  very slowly. For instance, the difference between  $\nu_{\text{SAW}}$  and  $\nu_{All}$  is reduced to 0.01, i.e.,  $\nu_{All} = 0.587$ , if the maximum segment number  $N$  is very large such as  $N = 10^8$ . Here we remark that the power-law decay is considered as an approximate expression, since we have confirmed it only over a decade from  $N = 300$  to 3,000.

For any other topological condition  $K$  than no topological constraint ( $All$ ) such as being topologically equivalent to a knot  $K$ , it is not practically easy to show numerically how the effective scaling exponent  $\nu_K$  for the cylindrical SAP with a small nonzero radius  $r_{\text{ex}}$  approaches  $\nu_{\text{SAW}}$  as the maximum segment number  $N$  increases.

However, from Figures 5 and 6 we argue that the effective scaling exponent  $\nu_K$  of the cylindrical SAP with any given knot  $K$  approaches the scaling exponent of SAW  $\nu_{\text{SAW}}$  if the maximum segment number  $N$  becomes very large. The way it approaches  $\nu_{\text{SAW}}$  can be very slow such as that it approaches 0.587 (i.e. the difference from  $\nu_{\text{SAW}}$  is given by 0.01) when the maximum of  $N$  is as large as  $N = 10^8$  or larger.

In Figure 5 we observe that the estimates of effective scaling exponents  $\nu_K$  for several knots  $K$  are all larger than the estimate of  $\nu_{All}$  for almost any value of radius  $r_{\text{ex}}$ . We thus expect that the effective exponents  $\nu_K$  are larger than  $\nu_{All}$  for any value of cylindrical radius  $r_{\text{ex}}$  even if the maximum of  $N$  becomes extremely large. Thus, if the maximum segment number  $N$  becomes very large, the effective scaling exponent  $\nu_K$  for the cylindrical SAP of a knot  $K$  even with a small radius  $r_{\text{ex}}$  approaches the value of  $\nu_{\text{SAW}}$  very closely, since  $\nu_{All}$  increases to  $\nu_{\text{SAW}}$  and  $\nu_K$  is assumed to be larger than  $\nu_{All}$ .

We now argue enhancement of the effective scaling exponent  $\nu_K$  of the RP with a knot  $K$ . It follows from the continuity conjecture of effective exponents  $\nu_K$  with respect to radius  $r_{\text{ex}}$  shown in section 5.1 that the effective scaling exponent  $\nu_K$  of the equilateral RP with a knot  $K$  approaches  $\nu_{\text{SAW}}$  if the upper limit in the

plot range of  $N$  (i.e., the maximum of  $N$ ) goes to infinity. We expect that the difference  $\nu_{\text{SAW}} - \nu_K$  is smaller than 0.01 if the maximum of  $N$  is given by  $10^8$ . If the estimate of  $\nu_K$  at  $r_{\text{ex}} = 0.005$  becomes equal to  $\nu_{\text{SAW}}$ , the estimate of  $\nu_K$  at  $r_{\text{ex}} = 0.0$  becomes also equal to it, since the effective exponent  $\nu_K$  is assumed to be continuous with respect to radius  $r_{\text{ex}}$ .

We give a conclusion to the above argument: The effective scaling exponent  $\nu_K$  of the RP with a fixed knot  $K$  should approach the value of  $\nu_{\text{SAW}}$  if the upper limit in the plot range of segment number  $N$  is very large such as  $N = 10^8$ . However, the topological finite-size effect is very strong, so that it is effectively smaller than the value of  $\nu_{\text{SAW}}$  if segment number  $N$  is less than  $10^4$ .

## 6 Additivity of equilibrium lengths for composite knots

### 6.1 Equilibrium lengths of composite knots

Associated with topological swelling we propose the following conjecture: If the equilibrium lengths for knot  $K_j$  are given by  $N_{\text{eq}}(K_j)$  for  $j = 1$  and  $2$ , respectively, then the equilibrium length for the composite knot  $K_1\#K_2$ , denoted by  $N_{\text{eq}}(K_1\#K_2)$ , is given by the sum

$$N_{\text{eq}}(K_1\#K_2) = N_{\text{eq}}(K_1) + N_{\text{eq}}(K_2). \quad (9)$$

$r_{\text{ex}}$	$3_1\#3_1$	$3_1\#4_1$	$3_1\#3_1\#3_1$	$3_1\#3_1\#4_1$	$3_1\#4_1\#4_1$
0.0	$325 \pm 19$	$405 \pm 33$	$442 \pm 29$	$528 \pm 51$	$621 \pm 76$
Fraction	$0.82 \pm 0.05$	$0.83 \pm 0.07$	$0.75 \pm 0.05$	$0.77 \pm 0.07$	$0.80 \pm 0.10$
0.01	$654 \pm 30$	$900 \pm 57$	$943 \pm 72$	$1167 \pm 97$	$1426 \pm 251$
Fraction	$0.93 \pm 0.04$	$0.94 \pm 0.06$	$0.89 \pm 0.07$	$0.89 \pm 0.07$	$0.92 \pm 0.16$
0.02	$1244 \pm 51$	$1740 \pm 115$	$1743 \pm 98$	$2272 \pm 179$	$2717 \pm 587$
Fraction	$0.99 \pm 0.04$	$1.00 \pm 0.07$	$0.93 \pm 0.05$	$0.96 \pm 0.08$	$0.95 \pm 0.20$
0.03	$2081 \pm 71$	$2696 \pm 167$	$2907 \pm 230$	$3951 \pm 450$	$4468 \pm 894$
Fraction	$1.00 \pm 0.03$	$0.88 \pm 0.05$	$0.94 \pm 0.07$	$0.96 \pm 0.11$	$0.88 \pm 0.18$
0.04	$3217 \pm 85$	$4430 \pm 323$	$4655 \pm 317$	$5821 \pm 687$	$7757 \pm 2187$
Fraction	$1.00 \pm 0.03$	$0.90 \pm 0.07$	$0.96 \pm 0.07$	$0.89 \pm 0.11$	$0.95 \pm 0.27$
0.05	$4869 \pm 168$	$6452 \pm 413$	$7053 \pm 564$	$10203 \pm 1245$	$14339 \pm 2882$
Fraction	$1.00 \pm 0.03$	$0.86 \pm 0.06$	$0.99 \pm 0.08$	$1.03 \pm 0.13$	$1.14 \pm 0.23$

Table 6: Equilibrium lengths for composite knots of knots  $3_1$  and  $4_1$ . Fraction shows the ratio of the equilibrium length of a composite knot to the sum of the equilibrium lengths over all the constituent prime knots together with errors.

For an illustration, let us confirm the conjecture for composite knot  $3_1\#4_1$  numerically by making use of the best estimates for the parameters of the formula of eq (1). For  $r_{\text{ex}} = 0.02$  the ratio of topological swelling for the trefoil knot ( $3_1$ ) becomes 1.0 at  $N = 626$  and for the figure-eight knot ( $4_1$ ) at  $N = 1119$ , while that of composite knot  $3_1\#4_1$  at  $N = 1740$ . It is almost equal to the sum of the numbers  $N_1 = 626$  and  $N_2 = 1119$ , which is given by 1745. Thus, the ratio of the

equilibrium length of the composite knot  $3_1\#4_1$  to the sum of those of knots  $3_1$  and  $4_1$  is given by 1.0 with respect to errors.

Several examples support numerically the additivity conjecture. In Table 6 the estimates of the equilibrium length for five composite knots are listed for several different values of radius  $r_{\text{ex}}$  of cylindrical segments. In each row of a given value of radius  $r_{\text{ex}}$  the row of ‘‘Fraction’’ shows the ratio of the equilibrium length of a given composite knot,  $N_{\text{eq}}(\sum_j \#K_j)$ , which we denote simply by  $N_{12}$ , to the sum of the equilibrium lengths of all constituent prime knots,  $\sum_j N_{\text{eq}}(K_j)$ , which we denote simply by  $N_1 + N_2$ . The fraction is denoted by  $N_{12}/(N_1 + N_2)$ . They are close to 1.0 with respect to errors at least for SAP.

## 6.2 Additivity compatible with the local knot conjecture

Let us now argue that the additivity of equilibrium lengths for composite knots is compatible and even consistent with the local knot conjecture. The conjecture is given as follows. In an ensemble of such RP or SAP with a fixed prime knot the majority of them have such knotted regions that are localized along the polygonal chains [35, 36, 37]. In a given SAP with a prime knot  $K$ , if the knotted region is localized as in the local knot conjecture, we can take a subchain which corresponds to the knotted region. We call the subchain a locally knotted SAW with the knot  $K$ , which consists of SAW with the local knot  $K$  on it. We also assume that if we connect the two ends of a locally knotted SAW with a knot  $K$ , we have SAP with the knot  $K$ . Under the local knot conjecture we expect that the majority of SAPs with a knot  $K$  have locally knotted SAW with the knot  $K$  as subchains of the SAP.

Recall that if the equilibrium length for a knot  $K$  is given by  $N$ , the mean-square radius of gyration of SAP with the fixed knot  $K$  is equal to that of SAP under no topological constraint. Here, we physically interpret that topological entropic repulsions are balanced with the complexity of the knot  $K$  in the SAP with the knot  $K$  of  $N$  segments. Thus, also in  $N$ -step locally knotted SAWs with the knot  $K$ , we say that topological entropic repulsions are balanced with the complexity of the knot  $K$  if the step number  $N$  is equal to the equilibrium length for the knot  $K$ .

Suppose that in a SAP with a prime knot  $K_1$  of  $N_1$  segments topological entropic repulsions are balanced with the complexity of the knot  $K_1$  and also that in a SAP with a prime knot  $K_2$  of  $N_2$  segments topological entropic repulsions are balanced with the complexity of the knot  $K_2$ . According to the local knot conjecture, in the locally knotted  $N_j$ -step SAWs with the knot  $K_j$  topological entropic repulsions are balanced with the complexity of the knot  $K_j$  for  $j = 1$  and 2, respectively. We then suggest that the topological entropic repulsions in the SAP of  $N_1 + N_2$  segments with the composite knot  $K_1\#K_2$  should be balanced with the complexity of the knot  $K_1\#K_2$ . Here, we expect that in the composite SAW of  $N_1 + N_2$  steps with the composite knot  $K_1\#K_2$  there are two locally knotted regions which correspond to the two prime knots  $K_1$  and  $K_2$ , respectively. Since in each of the  $N_j$ -step locally knotted SAWs ( $j = 1, 2$ ) the topological entropic repulsions are balanced with the knot complexity of the knot  $K_j$ , the whole topological entropic repulsions in the composite SAW of  $N_1 + N_2$  steps with the knot  $K_1\#K_2$  should be balanced with the complexity of the knot

$K_1\#K_2$ . Under the local knot conjecture it follows that the equilibrium length of the total SAP of  $N_1 + N_2$  segments with the knot  $K_1\#K_2$  is given by the sum  $N_1 + N_2$ .

### 6.3 Possibility of knots in RP being less localized than in SAP

We now argue that the local knot conjecture holds for SAP well, while it holds for RP less than for SAP. In Table 6 we observe that the fractions  $N_{12}/(N_1 + N_2)$  are given from 0.9 to 1.0 for SAP, while it is about 0.8 for RP. They are smaller in RP than in SAP for the five composite knots. Here we expect that if knots are truly localized, then the fraction  $N_{12}/(N_1 + N_2)$  should be given by 1.0. We therefore suggest that the knotted region in the RP with a fixed knot is less localized than in the SAP with a fixed knot.

We recall that in Figure 4 the ratio of topological swelling in the equilateral RP,  $\langle R_g^2 \rangle_K / \langle R_g^2 \rangle_{All}$ , is plotted against the number of segments  $N$  for the six knots.

We suggest that topological entropic repulsions are stronger in knotted RP than in knotted SAP. If knotted regions are less localized in knotted RP than in knotted SAP, they should be more entangled in knotted RP and hence the topological entropic repulsions among segments should be stronger in knotted RP than in knotted SAP.

It may explain the reason why the fractions  $N_{12}/(N_1 + N_2)$  are smaller in knotted RP than those of knotted SAP. If topological entropic repulsions among segments are stronger in knotted RP, then the equilibrium length of a knot is smaller in RP than in SAP with respect to the characteristic length  $N_0$  which gives the scale of topological effects. Thus, when entropic repulsions are balanced with the knot complexity for a composite knot  $K_1\#K_2$ , the equilibrium length  $N_{12}$  is smaller in RP than in SAP, and hence we have smaller fractions  $N_{12}/(N_1 + N_2)$ .

## 7 Concluding remarks

For topological swelling of the RP with a fixed knot  $K$  we have argued that the topological finite-size effect plays a central role in the mean-square radius of gyration of the RP under the topological constraint  $K$  plotted against segment number  $N$ .

We have shown that the three-parameter formula (7) with scaling exponent as a fitting parameter gives a good fitted curve to the plot of the mean-square gyration radius of the cylindrical SAP with a fixed knot against segment number  $N$  for any given value of radius  $r_{ex}$ . The results should be useful for describing the mean-square radius of gyration for knotted semi-flexible ring polymers.

We have argued that the effective scaling exponent of the RP with a knot  $K$  is given by the scaling exponent of SAW  $\nu_{SAW}$  if the upper limit of the plot range of  $N$  becomes infinitely large such as  $N = 10^8$  or larger than that. However, if the upper limit of  $N$  is given by a finite number such as  $N = 10^4$ , it is definitely less than  $\nu_{SAW}$  with respect to errors.

It follows that, at least for segment numbers  $N$  less than  $10^4$ , to the plots of the mean-square radius of gyration for the RP under a topological constraint against segment number  $N$  it is impossible to apply such a large- $N$  asymptotic expansion that would have the effective scaling exponent equal to the scaling

exponent of SAW and give good theoretical curves with small  $\chi^2$  values where there are only three fitting parameters.

We have shown that the equilibrium length of a composite knot is approximately equal to the sum of those of constituent prime knots of which the composite knot consists. Furthermore, we have argued that the additivity of equilibrium lengths for composite knots is compatible with the local knot conjecture.

## Acknowledgements

The authors would like to thank T. Prellberg for helpful comments. They are also thankful for comments to many participants in the Conference on Means, Methods and Results in the Statistical Mechanics of Polymeric Systems II, June 12 -14, 2017, The Fields Institute, Toronto, Canada. The present research is partially supported by the Grant-in-Aid for Scientific Research No. 26310206.



# S1 Ratio of topological swelling for the figure-eight knot

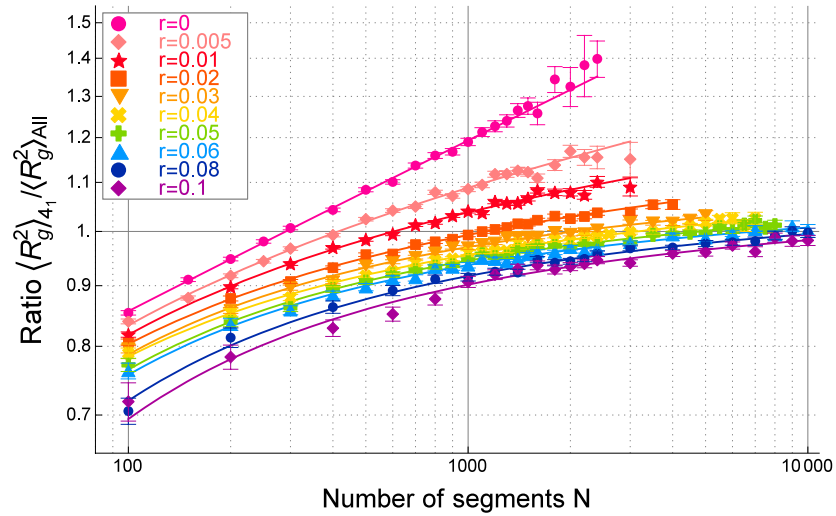


Figure S1: Ratio of topological swelling for the figure-eight knot ( $4_1$ ) in the cylindrical SAP with radius  $r_{ex}$ ,  $\langle R_g^2 \rangle_{4_1} / \langle R_g^2 \rangle_{All}$ , plotted against the number of segments  $N$  in the double-logarithmic scale.

$r_{ex}$	$a_K$	$\Delta\nu_K$	$b_K$	$\chi^2/\text{DF}$
0	$0.454 \pm 0.026$	$0.0702 \pm 0.0036$	$-0.12 \pm 0.25$	0.69
0.005	$0.753 \pm 0.044$	$0.0306 \pm 0.0037$	$-1.65 \pm 0.24$	1.81
0.01	$0.869 \pm 0.037$	$0.0175 \pm 0.0027$	$-1.99 \pm 0.18$	1.31
0.02	$0.913 \pm 0.026$	$0.0110 \pm 0.0017$	$-2.04 \pm 0.14$	0.89
0.03	$0.981 \pm 0.030$	$0.0047 \pm 0.0018$	$-2.31 \pm 0.16$	1.24
0.04	$0.936 \pm 0.022$	$0.0065 \pm 0.0013$	$-2.11 \pm 0.13$	0.75
0.05	$0.963 \pm 0.025$	$0.0043 \pm 0.0014$	$-2.37 \pm 0.16$	0.95
0.06	$0.960 \pm 0.025$	$0.0039 \pm 0.0015$	$-2.40 \pm 0.17$	0.81
0.08	$0.942 \pm 0.031$	$0.0044 \pm 0.0018$	$-2.66 \pm 0.22$	0.67
0.1	$0.930 \pm 0.049$	$0.0046 \pm 0.0029$	$-2.84 \pm 0.37$	1.00

Table S1: Best estimates of the parameters in eq (1) for the ratio of the mean-square radius of gyration for the cylindrical SAP with the figure-eight knot  $4_1$  to that of no topological constraint, denoted by  $\langle R_g^2 \rangle_{4_1} / \langle R_g^2 \rangle_{All}$ .

## S2 Gyration radius of SAP with a fixed knot

$r_{\text{ex}}$	$A_K$	$\nu_K$	$B_K$	$\chi^2/\text{DF}$
Knot $0_1$				
0	$0.0342 \pm 0.0013$	$0.5743 \pm 0.0024$	$3.17 \pm 0.22$	0.72
0.005	$0.0376 \pm 0.0010$	$0.5749 \pm 0.0017$	$2.41 \pm 0.15$	1.00
0.01	$0.03779 \pm 0.00073$	$0.5794 \pm 0.0012$	$2.30 \pm 0.11$	0.83
0.02	$0.03987 \pm 0.00046$	$0.5837 \pm 0.0007$	$1.931 \pm 0.066$	0.73
0.03	$0.04154 \pm 0.00051$	$0.58710 \pm 0.00073$	$1.709 \pm 0.071$	1.59
0.04	$0.04447 \pm 0.00033$	$0.58763 \pm 0.00043$	$1.419 \pm 0.043$	1.07
0.05	$0.04697 \pm 0.00023$	$0.58841 \pm 0.00028$	$1.197 \pm 0.029$	0.70
0.06	$0.05029 \pm 0.00027$	$0.58783 \pm 0.00031$	$0.928 \pm 0.032$	1.20
Knot $3_1$				
0	$0.0421 \pm 0.0013$	$0.5635 \pm 0.0020$	$0.25 \pm 0.14$	0.92
0.005	$0.0408 \pm 0.0010$	$0.5715 \pm 0.0016$	$0.25 \pm 0.13$	1.15
0.01	$0.04109 \pm 0.00077$	$0.5761 \pm 0.0011$	$0.106 \pm 0.097$	0.89
0.02	$0.04301 \pm 0.00086$	$0.5807 \pm 0.0012$	$-0.21 \pm 0.11$	1.70
0.03	$0.04565 \pm 0.00050$	$0.5827 \pm 0.00064$	$-0.490 \pm 0.065$	0.76
0.04	$0.04839 \pm 0.00037$	$0.58391 \pm 0.00044$	$-0.779 \pm 0.049$	0.57
0.05	$0.05091 \pm 0.00053$	$0.5849 \pm 0.00057$	$-1.026 \pm 0.070$	1.19
0.06	$0.05269 \pm 0.00044$	$0.58621 \pm 0.00046$	$-1.154 \pm 0.060$	0.85
Knot $4_1$				
0	$0.0368 \pm 0.0022$	$0.5717 \pm 0.0038$	$0.13 \pm 0.27$	0.69
0.005	$0.0394 \pm 0.0025$	$0.5741 \pm 0.0040$	$-0.46 \pm 0.30$	1.64
0.01	$0.0401 \pm 0.0021$	$0.5776 \pm 0.0033$	$-0.63 \pm 0.26$	1.46
0.02	$0.0404 \pm 0.0014$	$0.5846 \pm 0.0021$	$-0.76 \pm 0.19$	0.86
0.03	$0.0443 \pm 0.0017$	$0.5845 \pm 0.0022$	$-1.22 \pm 0.21$	1.27
0.04	$0.0438 \pm 0.0012$	$0.5895 \pm 0.0015$	$-1.11 \pm 0.17$	0.76
0.05	$0.0475 \pm 0.0013$	$0.5887 \pm 0.0015$	$-1.59 \pm 0.18$	0.93
0.06	$0.0501 \pm 0.0013$	$0.5889 \pm 0.0014$	$-1.78 \pm 0.17$	0.75

Table S2: Best estimates of the parameters of eq (7) for knots  $0_1$ ,  $3_1$  and  $4_1$ .

$r_{\text{ex}}$	$A_K$	$\nu_K$	$B_K$	$\chi^2/\text{DF}$
Knot $5_1$				
0	$0.0371 \pm 0.0049$	$0.5706 \pm 0.0084$	$-0.62 \pm 0.56$	1.38
0.005	$0.0373 \pm 0.0034$	$0.5768 \pm 0.0057$	$-0.75 \pm 0.41$	1.05
0.01	$0.0315 \pm 0.0028$	$0.5917 \pm 0.0054$	$0.04 \pm 0.46$	0.93
0.02	$0.0395 \pm 0.0030$	$0.5858 \pm 0.0046$	$-1.34 \pm 0.38$	1.13
0.03	$0.0426 \pm 0.0032$	$0.5871 \pm 0.0044$	$-1.79 \pm 0.40$	1.13
0.04	$0.0408 \pm 0.0027$	$0.5938 \pm 0.0037$	$-1.56 \pm 0.41$	0.93
0.05	$0.0434 \pm 0.0030$	$0.5936 \pm 0.0038$	$-1.66 \pm 0.47$	0.86
0.06	$0.0415 \pm 0.0026$	$0.5991 \pm 0.0034$	$-1.48 \pm 0.47$	0.58
Knot $5_2$				
0	$0.0313 \pm 0.0025$	$0.5819 \pm 0.0052$	$0.12 \pm 0.38$	0.74
0.005	$0.0371 \pm 0.0022$	$0.5769 \pm 0.0037$	$-0.76 \pm 0.27$	0.77
0.01	$0.0360 \pm 0.0013$	$0.5843 \pm 0.0023$	$-0.84 \pm 0.18$	0.35
0.02	$0.0370 \pm 0.0022$	$0.5892 \pm 0.0036$	$-0.93 \pm 0.31$	1.06
0.03	$0.0370 \pm 0.0018$	$0.5949 \pm 0.0029$	$-1.06 \pm 0.28$	0.72
0.04	$0.0434 \pm 0.0024$	$0.5901 \pm 0.0031$	$-1.93 \pm 0.33$	1.14
0.05	$0.0476 \pm 0.0020$	$0.5882 \pm 0.0023$	$-2.38 \pm 0.25$	0.70
0.06	$0.0458 \pm 0.0027$	$0.5935 \pm 0.0032$	$-2.09 \pm 0.41$	1.11

Table S3: Best estimates of the parameters of eq (7) for knots  $5_1$  and  $5_2$ .

$r_{\text{ex}}$	$A_K$	$\nu_K$	$B_K$	$\chi^2/\text{DF}$
Knot $3_1\#3_1$				
0	$0.0404 \pm 0.0020$	$0.5667 \pm 0.0031$	$-0.78 \pm 0.23$	1.24
0.005	$0.0422 \pm 0.0014$	$0.5704 \pm 0.0021$	$-1.17 \pm 0.17$	1.09
0.01	$0.0415 \pm 0.0016$	$0.5762 \pm 0.0022$	$-1.19 \pm 0.21$	1.42
0.02	$0.0438 \pm 0.0015$	$0.580 \pm 0.002$	$-1.47 \pm 0.22$	1.41
0.03	$0.0458 \pm 0.0013$	$0.5831 \pm 0.0015$	$-1.79 \pm 0.19$	0.99
0.04	$0.0500 \pm 0.0011$	$0.5826 \pm 0.0012$	$-2.22 \pm 0.17$	0.83
0.05	$0.0521 \pm 0.0015$	$0.5841 \pm 0.0015$	$-2.48 \pm 0.24$	1.19
0.06	$0.0542 \pm 0.0014$	$0.5851 \pm 0.0013$	$-2.70 \pm 0.23$	0.79
Knot $3_1\#4_1$				
0	$0.0382 \pm 0.0026$	$0.5707 \pm 0.0042$	$-1.29 \pm 0.30$	0.99
0.005	$0.0395 \pm 0.0013$	$0.5744 \pm 0.0020$	$-1.54 \pm 0.16$	0.40
0.01	$0.038 \pm 0.002$	$0.5814 \pm 0.0030$	$-1.44 \pm 0.28$	0.87
0.02	$0.0399 \pm 0.0022$	$0.5856 \pm 0.0031$	$-1.74 \pm 0.33$	0.95
0.03	$0.0385 \pm 0.0020$	$0.5930 \pm 0.0029$	$-1.41 \pm 0.37$	0.81
0.04	$0.0407 \pm 0.0025$	$0.5939 \pm 0.0033$	$-1.71 \pm 0.49$	1.17
0.05	$0.0482 \pm 0.0026$	$0.5885 \pm 0.0028$	$-2.89 \pm 0.43$	0.86
0.06	$0.0513 \pm 0.0029$	$0.5880 \pm 0.0029$	$-3.17 \pm 0.49$	0.75

Table S4: Best estimates of the parameters of eq (7) for the composite knots  $3_1\#3_1$  and  $3_1\#4_1$ .

$r_{\text{ex}}$	$A_K$	$\nu_K$	$B_K$	$\chi^2/\text{DF}$
0	$0.0467 \pm 0.0026$	$0.5589 \pm 0.0034$	$-2.67 \pm 0.25$	0.97
0.005	$0.0393 \pm 0.0021$	$0.5756 \pm 0.0031$	$-2.13 \pm 0.28$	0.96
0.01	$0.0442 \pm 0.0028$	$0.5733 \pm 0.0036$	$-2.71 \pm 0.37$	1.39
0.02	$0.0464 \pm 0.0022$	$0.5778 \pm 0.0026$	$-3.10 \pm 0.33$	1.00
0.03	$0.0454 \pm 0.0030$	$0.5839 \pm 0.0035$	$-2.63 \pm 0.53$	1.45
0.04	$0.0522 \pm 0.0030$	$0.581 \pm 0.003$	$-3.87 \pm 0.48$	1.23
0.05	$0.0525 \pm 0.0035$	$0.5841 \pm 0.0034$	$-3.71 \pm 0.62$	1.02
0.06	$0.0563 \pm 0.0040$	$0.5834 \pm 0.0035$	$-4.11 \pm 0.69$	0.80
0.08	$0.059 \pm 0.015$	$0.586 \pm 0.013$	$-4.0 \pm 2.8$	1.17
0.1	$0.037 \pm 0.02$	$0.613 \pm 0.026$	$1.8 \pm 7.3$	0.65

Table S5: Best estimates of the parameters of eq (7) for knot  $3_1\#3_1\#3_1$ .

$r_{\text{ex}}$	$A_K$	$\nu_K$	$B_K$	$\chi^2/\text{DF}$
0	$0.0357 \pm 0.0029$	$0.5751 \pm 0.0048$	$-2.02 \pm 0.39$	0.96
0.005	$0.0370 \pm 0.0035$	$0.5783 \pm 0.0055$	$-2.15 \pm 0.51$	1.60
0.01	$0.0431 \pm 0.0030$	$0.5746 \pm 0.0040$	$-3.12 \pm 0.40$	0.84
0.02	$0.0437 \pm 0.0029$	$0.5811 \pm 0.0036$	$-3.39 \pm 0.45$	0.90
0.03	$0.0463 \pm 0.0044$	$0.583 \pm 0.005$	$-3.66 \pm 0.72$	1.14
0.04	$0.0434 \pm 0.0043$	$0.5905 \pm 0.0051$	$-2.91 \pm 0.87$	0.86
0.05	$0.0540 \pm 0.0055$	$0.5827 \pm 0.0052$	$-4.77 \pm 0.90$	0.81
0.06	$0.0471 \pm 0.0072$	$0.5929 \pm 0.0076$	$-3.8 \pm 1.5$	0.96
0.08	$0.089 \pm 0.019$	$0.567 \pm 0.011$	$-10.45 \pm 0.94$	2.23

Table S6: Best estimates of the parameters of eq (7) for knot  $3_1\#3_1\#4_1$ .

$r_{\text{ex}}$	$A_K$	$\nu_K$	$B_K$	$\chi^2/\text{DF}$
0	$0.0403 \pm 0.0041$	$0.5670 \pm 0.0062$	$-3.12 \pm 0.44$	0.48
0.005	$0.0240 \pm 0.0044$	$0.604 \pm 0.011$	$-0.40 \pm 1.2$	0.85
0.01	$0.0597 \pm 0.0088$	$0.5554 \pm 0.0086$	$-5.33 \pm 0.72$	1.13
0.02	$0.0338 \pm 0.0061$	$0.5955 \pm 0.0097$	$-2.5 \pm 1.3$	0.67
0.03	$0.0587 \pm 0.0098$	$0.5712 \pm 0.0091$	$-6.4 \pm 1.1$	1.00
0.04	$0.051 \pm 0.012$	$0.582 \pm 0.012$	$-4.6 \pm 1.8$	0.91
0.05	$0.0495 \pm 0.0083$	$0.5869 \pm 0.0091$	$-4.84 \pm 0.90$	0.99
0.06	$0.166 \pm 0.053$	$0.530 \pm 0.017$	$-15.3 \pm 1.9$	0.79
0.08	$0.070 \pm 0.049$	$0.580 \pm 0.036$	$-12.7 \pm 4.7$	0.50

Table S7: Best estimates of the parameters of eq (7) for knot  $3_1\#4_1\#4_1$ .

### S3 Best estimates to the plots of the mean-square gyration radius for cylindrical SAP of no topological constraint versus segment number

By applying eq (7) in the case of  $K = all$  we derive the fitted curves to the plots of the mean-square radius of gyration for the cylindrical SAP under no topological constraint  $\langle R_g^2 \rangle_{All}$  against the number of segments  $N$  for several different values of cylindrical radius  $r_{ex}$ . The curves fit to the data points very well and the  $\chi^2$  values per DF are less than 2.0 for almost all the values of cylindrical radius  $r_{ex}$ . The best estimates of the parameters are listed in Table S8.

Moreover, the absolute value of the coefficient of the finite-size correction term  $B_{All}$  is less than 1.0 for the large values of cylindrical radius satisfying  $r_{ex} \geq 0.06$ , as listed in Table S8. Therefore, for  $N > 10^3$ , the finite-size correction term is very small such as less than 3 percentages in the case of the large values of the cylindrical radius with  $r_{ex} \geq 0.06$ .

$r_{ex}$	$A_{All}$	$\nu_{All}$	$B_{All}$	$\chi^2/DF$
0	$0.08106 \pm 0.00067$	$0.50148 \pm 0.00049$	$0.253 \pm 0.045$	1.72
0.005	$0.04610 \pm 0.00071$	$0.55084 \pm 0.0009$	$2.138 \pm 0.098$	3.83
0.01	$0.04104 \pm 0.00048$	$0.56652 \pm 0.00067$	$2.379 \pm 0.076$	2.15
0.02	$0.04018 \pm 0.00043$	$0.57886 \pm 0.0006$	$2.160 \pm 0.071$	3.14
0.03	$0.04279 \pm 0.00025$	$0.58251 \pm 0.00034$	$1.718 \pm 0.039$	1.39
0.04	$0.04502 \pm 0.00018$	$0.58505 \pm 0.00023$	$1.460 \pm 0.027$	0.93
0.05	$0.04776 \pm 0.00012$	$0.58610 \pm 0.00014$	$1.184 \pm 0.017$	0.47
0.06	$0.0506 \pm 0.0002$	$0.58650 \pm 0.00022$	$0.956 \pm 0.025$	1.09
0.08	$0.05553 \pm 0.00019$	$0.58739 \pm 0.00019$	$0.654 \pm 0.020$	0.70
0.1	$0.0608 \pm 0.00026$	$0.58738 \pm 0.00025$	$0.351 \pm 0.026$	1.27

Table S8: Best estimates of the parameters in eq (7) for  $K = all$  to the plots of the mean-square radius of gyration of the cylindrical SAP under no topological constraint, i.e., that of all knots,  $\langle R_g^2 \rangle_{All}$ , against segment number  $N$ .

## References

- [1] Kramers, H. A. The Behavior of Macromolecules in Inhomogeneous Flow. *J. Chem. Phys.* **1946**, *14*, 415-424.
- [2] *Cyclic Polymers*, ed. Semlyen, J. A. Elsevier Applied Science Publishers: New York, 1986; 2nd Ed. Kluwer Academic Publ.: Dordrecht, 2000.
- [3] Bates, A. D.; Maxwell, A. *DNA Topology*; Oxford Univ. Press, 2005.
- [4] Vinograd, J.; Lebowitz, J.; Radloff, R.; Watson, R.; Laipis, P. The twisted circular form of polyoma viral DNA. *Proc. Natl. Acad. Sci. (U.S.)* **1965**, *53*, 1104-1111.
- [5] Krasnow, M. A.; Stasiak, A.; Spengler, S. J.; Dean, F.; Koller, T.; Cozzarelli, N.R. Determination of the absolute handedness of knots and catenanes of DNA. *Nature* **1983**, *304*, 559-560.
- [6] Dean, F. B.; Stasiak, A.; Koller, T.; Cozzarelli, N. R. Duplex DNA Knots Produced by *Escherichia coli* Topoisomerase I. *J. Biol. Chem.* **1985**, *260*, 4975-4983.
- [7] Taylor, W. R. A deeply knotted protein structure and how it might fold. *Nature* **2000**, *406*, 916-919.
- [8] Haglund, E.; Sulkowska, J. I.; Noel, J. K.; Lammert, H.; Onuchic, J. N.; Jennings, P. A. Pierced Lasso Bundles Are a New Class of Knot-like Motifs. *PLoS Computational Biology* **2014**, *10*(6), 1003613.
- [9] Craik, D. J. Seamless Proteins Tie Up Their Loose Ends. *Science* **2006**, *311*, 1563-1564.
- [10] Rybenkov, V. V.; Cozzarelli, N. R.; and Vologodskii, A. V. Probability of DNA knotting and the effective diameter of the DNA double helix. *Proc. Natl. Acad. Sci. USA* **1993**, *90*, 5307-5311.
- [11] Shaw, S. Y.; Wang, J. C. Knotting of a DNA Chain During Ring Closure. *Science* **1993**, *260*, 533-536.
- [12] Plesa, C.; Daniel Verschuere, D.; Pud, S.; van der Torre, J.; Ruitenber, J. W.; Witteveen, M. J.; Jonsson, M. P.; Grosberg, A. Y.; Rabin, Y.; Dekker, C. Direct observation of DNA knots using a solid-state nanopore. *Nature Nanotech.* **2016**, *11*, 1093-1097.
- [13] Danon, J. J.; Krüger, A.; Leigh, D. A.; Lemonnier, J.-F.; Stephens, A. J.; Vitorica-Yrezabal, I. J.; Woltering, S. L. Braiding a molecular knot with eight crossings. *Science* **2017**, *355*, 159-162.
- [14] Oike, H.; Imaizumi, H.; Mouri, T.; Yoshioka, Y.; Uchibori, A.; Tezuka, Y. Designing Unusual Polymer Topologies by Electrostatic Self-Assembly and Covalent Fixation. *J. Am. Chem. Soc.* **2000**, *122*, 9592-9599.
- [15] Bielawski, C. W.; Benitez, D.; Grubbs, R. H. An "Endless" Route to Cyclic Polymers. *Science* **2002**, *297*, 2041-2044.
- [16] Cho, D.; Masuoka, K.; Koguchi, K.; Asari, T.; Kawaguchi, D.; Takano, A.; Matsushita, Y. Preparation and Characterization of Cyclic Polystyrenes. *Polymer Journal* **2005**, *37*, 506-511.

- [17] Takano, A.; Kushida, Y.; Aoki, K.; Masuoka, K.; Hayashida, K.; Cho, D.; Kawaguchi, D.; Matsushita, Y. HPLC Characterization of Cyclization Reaction Product Obtained by End-to-End Ring Closure Reaction of a Telechelic Polystyrene. *Macromolecules* **2007**, *40*, 679-681.
- [18] Laurent, B. A.; Grayson, S. An Efficient Route to Well-Defined Macrocyclic Polymers via "Click" Cyclization. *J. Am. Chem. Soc.* **2006**, *128*, 4238-4239.
- [19] Sugai, N.; Heguri, H.; Yamamoto, T.; Tezuka, Y. Synthesis of Orientationally Isomeric Cyclic Stereoblock Poly lactides with Head-to-Head and Head-to-Tail Linkages of the Enantiomeric Segments. *ACS Macro Lett.* **2012**, *1*, 902-906.
- [20] *Topological Polymer Chemistry: Progress in cyclic polymers in syntheses, properties and functions*, ed. by Tezuka, Y. World Scientific Publ.: Singapore, 2013.
- [21] Deutsch, J. M. Equilibrium size of large ring molecules. *Phys. Rev. E* **1999**, *59*, R2539.
- [22] Grosberg, A. Y. Critical Exponents for Random Knots. *Phys. Rev. Lett.* **2000**, *85*, 3858-3861.
- [23] Shimamura, M. K.; and Deguchi, T. Anomalous finite-size effects for the mean-squared gyration radius of Gaussian random knots. *J. Phys. A: Math. Gen.* **2002**, *35*, L241-L246.
- [24] Dobay, A.; Dubochet, J.; Millett, K.; Sottas, P. E.; Stasiak, A.; Scaling behavior of random knots. *Proc. Natl. Acad. Sci. USA* **2003**, *100*, 5611-5615.
- [25] Matsuda, H.; Yao, A.; Tsukahara, H.; Deguchi, T.; Furuta, K.; Inami, T.; Average size of random polygons with fixed knot topology. *Phys. Rev. E* **2003**, *68*, 011102.
- [26] Moore, N. T.; Lua, R. C.; Grosberg, A. Y. Topologically driven swelling of a polymer loop. *Proc. Natl. Acad. Sci. USA* **2004**, *101*, 13431-13435.
- [27] Shimamura, M. K.; Deguchi, T. Gyration radius of a circular polymer under a topological constraint with excluded volume. *Phys. Rev. E* **2001**, *64*, 020801(R).
- [28] Shimamura, M. K.; Deguchi, T. Finite-size and asymptotic behaviors of the gyration radius of knotted cylindrical self-avoiding polygons. *Phys. Rev. E* **2002**, *65*, 051802.
- [29] Des Cloizeaux, J. Short range correlation between elements of a long polymer in a good solvent. *J. Physique* **1980**, *41*, 223-238.
- [30] Takano, A.; Ohta, Y.; Masuoka, K.; Matsubara, K.; Nakano, T.; Hino, A.; Itakura, M.; Takahashi, K.; Kinugasa, S.; Kawaguchi, D.; Takahashi, Y.; Matsushita, Y. Radii of Gyration of Ring-Shaped Polystyrenes with High Purity in Dilute Solutions. *Macromolecules* **2012**, *45*, 369-373.
- [31] Shimamura, M. K.; Deguchi, T. Characteristic length of random knotting for cylindrical self-avoiding polygons. *Phys. Lett. A* **2000**, *274*, 184-191.
- [32] Uehara, E.; Deguchi, T. Characteristic length of the knotting probability revisited. *J. Phys. Condens. Matter* **2015**, *27*, 354104



- [33] Rawdon, E.; Dobay, A.; Kern, J. C.; Millett, K. C.; Piatek, M.; Plunkett, P.; Stasiak, A. Scaling behavior and equilibrium lengths of knotted polymers. *Macromolecules* **2008**, *41*, 4444-4451.
- [34] Marcone, B.; Orlandini, E.; Stella, A. L.; Zonta, F. Size of knots in ring polymers. *Phys. Rev. E* **2007**, *75*, 041105.
- [35] Orlandini, E.; Tesi, M.C.; van Rensburg, E. J. J.; Whittington, S. G. Asymptotics of knotted lattice polygons. *J. Phys. A: Math. Gen.* **1998**, *31*, 5953-5967.
- [36] Katritch, V.; Olsen, W. K.; Vologodskii, A.; Dubochet, J.; Stasiak, A. Tightness of random knotting. *Phys. Rev. E* **2000**, *61*, 5545-5549.
- [37] Marcone, B.; Orlandini, E.; Stella, A. L.; Zonta, F. What is the length of a knot in a polygon? *J. Phys. A: Math. Gen.* **2005**, *38*, L15-L21.
- [38] Rosa, A.; Orlandini, E.; Tubiana, L.; Micheletti, C. Structure and Dynamics of Ring Polymers: Entanglement Effects Because of Solution Density and Ring Topology. *Macromolecules* **2011**, *44*, 8668-8680.
- [39] Murasugi, K.; Kurpita, B. *Knot Theory and Its Applications*; Birkhäuser: Boston, 1996.
- [40] Deguchi, T.; Tsurusaki, K.; A New Algorithm for Numerical Calculation of Link Invariants. *Phys. Lett. A* **1993**, *174* 29-37.
- [41] Polyak, M.; Viro, O. Gauss diagram formulas for Vassiliev invariants. *IMRN*. **1994**, *No. 11*, 445-453.
- [42] Deguchi, T.; Tsurusaki, K. A Statistical Study of Random Knotting Using the Vassiliev Invariants. *J. Knot Theory Ramif.* **1994**, *3*, 321-353.
- [43] Deguchi, T.; Tsurusaki, K. Universality of random knotting. *Phys. Rev. E*. **1997**, *55*, 6245-6248.
- [44] Le Guillou, J. C.; Zinn-Justin, J. Critical exponents from field theory. *Phys. Rev. B* **1980**, *21*, 3976-3998.
- [45] Nickel, B. G. One-Parameter Recursion Model for Flexible -Chain Polymers. *Macromolecules* **1991**, *24*, 1358-1365.
- [46] Li, B.; Madras, N.; Sokal, A. D. Critical Exponents, Hyperscaling, and Universal Amplitude Ratios for Two- and Three-Dimensional Self-Avoiding Walks. *J. Stat. Phys.* **1995**, *80*, 661-754.
- [47] Guida R.; Zinn-Justin, J. Critical exponents of the N-vector model. *J. Phys. A: Math. Gen.*, **1998**, *31*, 8103.
- [48] Clisby, N. Accurate Estimate of the Critical Exponent  $\nu$  for Self-Avoiding Walks via a Fast Implementation of the Pivot Algorithm. *Phys. Rev. Lett.* **2010**, *104*, 055702
- [49] Madras, N.; Slade, G. *Self-Avoiding Walks*; Birkhäuser: Boston, 1993.
- [50] Yamakawa, H. *Modern Theory of Polymer Solutions*; Harper and Row: New York, 1971.